Deconfined Quantum Criticality, Scaling Violations, and Classical Loop Models

Adam Nahum,[1] J. T. Chalker,[2] P. Serna,[2,3] M. Ortuño,[3] and A. M. Somoza[3]

[1]*Department of Physics, Massachusetts Institute of Technology, Cambridge, Massachusetts 02139, USA*
[2]*Theoretical Physics, Oxford University, 1 Keble Road, Oxford OX1 3NP, United Kingdom*
[3]*Departamento de Física—CIOyN, Universidad de Murcia, Murcia 30.071, Spain*

Numerical studies of the transition between Néel and valence bond solid phases in two-dimensional quantum antiferromagnets give strong evidence for the remarkable scenario of deconfined criticality, but display strong violations of finite-size scaling that are not yet understood. We show how to realize the universal physics of the Néel–valence-bond-solid (VBS) transition in a three-dimensional classical loop model (this model includes the subtle interference effect that suppresses hedgehog defects in the Néel order parameter). We use the loop model for simulations of unprecedentedly large systems (up to linear size $L = 512$). Our results are compatible with a continuous transition at which both Néel and VBS order parameters are critical, and we do not see conventional signs of first-order behavior. However, we show that the scaling violations are stronger than previously realized and are *incompatible* with conventional finite-size scaling, even if allowance is made for a weakly or marginally irrelevant scaling variable. In particular, different approaches to determining the anomalous dimensions η_{VBS} and $\eta_{\text{Néel}}$ yield very different results. The assumption of conventional finite-size scaling leads to estimates that drift to negative values at large sizes, in violation of the unitarity bounds. In contrast, the decay with distance of critical correlators on scales much smaller than system size is consistent with large positive anomalous dimensions. Barring an unexpected reversal in behavior at still larger sizes, this implies that the transition, if continuous, must show unconventional finite-size scaling, for example, from an additional dangerously irrelevant scaling variable. Another possibility is an anomalously weak first-order transition. By analyzing the renormalization group flows for the noncompact CP^{n-1} field theory (the n-component Abelian Higgs model) between two and four dimensions, we give the simplest scenario by which an anomalously weak first-order transition can arise without fine-tuning of the Hamiltonian.

I. INTRODUCTION

The paradigmatic "deconfined" quantum phase transition is that separating the Néel antiferromagnet from the columnar valence bond solid (VBS) for a square lattice of spin-1/2s. The theoretical arguments of Refs. [1–3] indicate that the Néel-VBS phase transition is described by the noncompact CP^1 (NCCP^1) model [4], a field theory with bosonic spinons $z = (z_1, z_2)$ coupled to a noncompact U(1) gauge field:

$$\mathcal{L} = |(\nabla - iA)z|^2 + \kappa(\nabla \times A)^2 + \mu|z|^2 + \lambda|z|^4. \quad (1)$$

This theory is defined in three-dimensional Euclidean spacetime; the Néel order parameter is proportional to $z^\dagger \vec{\sigma} z$, where $\vec{\sigma}$ are the Pauli matrices.

Numerical results for the J–Q model (the Heisenberg antiferromagnet supplemented with a four-spin interaction [5]) support the validity of this continuum description [6–11], as does work on the SU(n) generalization of the problem at large n [12–15]. Unfortunately, though, the existence of a continuous phase transition in both the NCCP^1 model and the SU(2) lattice magnets remains a vexed question. While simulations of the J–Q model are compatible with a direct continuous transition, they show strong violations of finite-size scaling [9,10,16,17]. These persist up to the largest system sizes studied so far and hamper the extraction of meaningful critical exponents [10]. Additionally, direct numerical studies of the lattice NCCP^1 field theory have disagreed as to whether the transition is continuous [4,18] or whether scaling violations similar to those seen in the lattice magnets should be interpreted as the initial stages of runaway flow to a first-order transition [19].

Are the scaling violations seen at the Néel-VBS transition indeed signs of a first-order transition, with an anomalously large correlation length [16,17,19], are they

due to the critical theory possessing a weakly irrelevant scaling variable [9,20,21], or do they indicate something more exotic? This issue remains controversial. Its relevance extends beyond quantum magnets since the critical behavior of the $NCCP^1$ model is important for various other fundamental problems in statistical mechanics. For example, this field theory is believed to describe the three-dimensional classical O(3) model when hedgehog defects are disallowed [4], as well as the columnar ordering transition in the classical dimer model on the cubic lattice [22–27]. [In the latter example, SU(2) symmetry is absent microscopically but argued to emerge at the critical point.] There is also numerical evidence that similar scaling violations afflict the SU(3) and SU(4) generalizations of the deconfined transition [10,28].

In this paper, we introduce a new model which is ideally suited for studying the universal features of the Néel-VBS transition and perform simulations on very large systems (of linear size up to 512 lattice spacings, and 640 for a few selected observables). We verify that the model shows the basic features expected from the $NCCP^1$ field theory [Eq. (1)]: an apparently continuous direct transition, with emergent U(1) symmetry for rotations of the VBS order parameter at the critical point. However, we show that scaling violations are even stronger than previously appreciated. Conventional finite-size scaling assumptions are not obeyed: The data cannot be made to show scaling collapse, and quantities that would normally be expected to be universal instead drift with system size. The larger sizes considered here show that these drifts are stronger than the logarithmic form conjectured previously [8,9].

In common with Ref. [10], we see a drift in finite-size estimates of critical exponents. We show that this is more drastic than previously apparent. Estimates of the anomalous dimensions of both the Néel and VBS order parameters, as extracted from the correlation functions $G(r)$ at distances r comparable with the system size (e.g., $r = L/2$), yield negative values at large sizes. Negative anomalous dimensions are ruled out for a conformally invariant critical point by the unitarity bounds [29,30]. This, together with the form of the drifts mentioned above, rules out a conventional continuous transition with conventional finite-size scaling.

On the other hand, the decay of $G(r)$ with r for $r \ll L$ appears consistent with the large positive anomalous dimensions suggested for a deconfined critical point. It is conceivable that the transition could be continuous but that conventional finite-size scaling could fail as a result of a dangerously irrelevant variable [28]. As we discuss, in this scenario correlators $G(r)$ with $1 \ll r \ll L$ would be expected to show the true positive anomalous dimensions, while correlators with r of order L would behave anomalously (as in, e.g., ϕ^4 theory above 4D [31]). The hypothetical dangerously irrelevant variable discussed here should not be confused with the much discussed $\mathbb{Z}_4$ anisotropy for the VBS order parameter (Sec. IV B), which is dangerously irrelevant in a different sense.

Therefore, unless there is a reversal of the drift in exponents at still larger sizes, which seems unlikely, there are two possibilities: Either the transition is continuous with unconventional finite-size scaling behavior (for example, as a result of a dangerously irrelevant scaling variable), or it is first order. We will discuss both possibilities but cannot rule out either. We do not see the conventional signs of a first-order transition, such as double-peaked probability distributions for the energy and other quantities.

On the other hand, an alternative hypothesis put forward previously—that the scaling violations are due simply to a weakly or marginally irrelevant scaling variable [8,9,20]— is *not* supported by our data. We also rule out any explanation in terms of unconventional dynamic scaling, i.e., deviations from dynamical exponent $z = 1$: Our model has $z = 1$ by construction since it is isotropic in three dimensions. This isotropy is also a convenient feature from the point of view of simulations.

Turning to theory, we analyze the topology of the renormalization group (RG) flows in the $NCCP^{n-1}$ model between two and four dimensions, in order to assess the possibility of an anomalously weak first-order transition. This analysis unifies what is known about this field theory in $4 - \epsilon$ dimensions, in $2 + \epsilon$ dimensions, and at large n, and extends previous partial results [32]. Treating n as continuously varying, we argue that in 3D, there is a universal value n_* below which the deconfined critical point disappears by merging with a tricritical point. The argument does not fix the value of n_*, which could be greater or smaller than 2, so it does not tell us whether the $NCCP^1$ model has a continuous transition. However, it does have the following consequences. If n_* happens to be greater than 2, there is a possible mechanism by which a very weak first-order transition can appear for a range of n values (i.e., a large correlation length can be obtained without the need for fine-tuning of the Hamiltonian). The argument also shows that n_* is greater than 1. This means that the inverted XY transition in the model with $n = 1$ is *not* analytically connected to the critical point in the large-n regime of the $NCCP^{n-1}$ model, contrary to assumptions made in previous work.

This picture for the RG flows also clarifies that the usual $2 + \epsilon$ expansion of the O(3) sigma model does not describe the conventional O(3) transition in 3D but rather the deconfined critical point (if it exists at $n = 2$). This is natural: Hedgehogs are crucial in determining the critical behavior of the O(3) model in 3D [4], and the $2 + \epsilon$ expansion presumably fails to account for them. The conclusion is also in line with the RG result that the $2 + \epsilon$ approach to the 3D O(M) model should fail when M is less than a universal value M_c, conjectured to be above 3, as a result of neglecting the topology of the sphere [33]. Interestingly, our best estimates for the correlation-length

exponent at the deconfined transition (Sec. IV E) are close to $\nu = 1/2$, smaller than most previous estimates but in good agreement with the $2 + \epsilon$ predictions (Sec. VI D).

Returning to lattice models, our numerical strategy is, instead of focusing on a simple two-dimensional quantum Hamiltonian, to construct a simple 3D classical model that is well adapted to large-scale Monte Carlo simulations. While the correspondence with classical lattice models in one dimension higher is a standard tool for studying quantum phase transitions, one might, at first glance, think that this tool is not available for deconfined criticality. This is because deconfinement relies crucially on the fact that the Euclidean action for the spins in $2 + 1$ dimensions— *unlike* the energy functional for a classical spin model in three dimensions—contains imaginary terms (Berry phases). The effect of these terms is to endow hedgehogs in the Néel order parameter with position-dependent complex fugacities [34–36]. After coarse-graining, this leads to a phase cancellation effect that suppresses hedgehogs [1–3].

Contrary to the naive expectation above, we show that the remarkable physics of deconfinement, including the suppression of hedgehogs by phase cancellation, is present in our 3D classical model. This model is formulated in terms of configurations of loops on a lattice and is a variant of the models of Refs. [37,38]. The loop configurations have positive Boltzmann weights, so they define a conventional classical statistical mechanics problem. However, the partition function can also be mapped to a lattice field theory for CP^{n-1} spins, and in this representation, the Boltzmann weights are *not* necessarily real. We show by a direct calculation that they include the complex hedgehog fugacities necessary for deconfined criticality.

The loop model introduced here has qualitative features in common with loop ensembles arising in worldline quantum Monte Carlo techniques for sign-problem free Hamiltonians such as the J–Q model [39] (see also Ref. [40]). However, direct simulation of a quantum Hamiltonian leads to an ensemble of worldlines in continuous imaginary time, whereas the loop model is an isotropic three-dimensional lattice model. This is a desirable feature for numerical simulations as it fixes an otherwise unknown velocity and eliminates a potentially significant source of corrections to scaling [41]. The geometric form of the model also motivates new observables—for example, we find it useful to consider some percolationlike observables such as the number of system-spanning strands and the fractal dimension of the loops.

II. LOOP MODEL

An astonishing variety of critical phenomena can be studied using classical loop gases. The present lattice model involves two species (colors) of loops, or n colors in the $SU(n)$ generalization. It has a phase in which infinite loops proliferate and one in which all loops are short. The

short-loop phase spontaneously breaks lattice symmetry because the system must choose between four symmetry-related ways to pack the short loops.

The transfer matrix for loop models of this kind gives a correspondence with a 2D quantum magnet on the square lattice [38]. The color of a strand is related to the state of the spin (at a given point in Euclidean space-time) in the quantum problem. The infinite-loop phase corresponds to the Néel phase: The presence of infinite loops is equivalent to the presence of long-range spin correlations. The four degenerate short-loop phases map to the four equivalent columnar VBS patterns on the square lattice. The schematic correspondence between the loop model and the continuum field theory [Eq. (1)] is that the two species of loops are worldlines of the two species of bosonic spinons (z_1, z_2). (See Sec. V for more details on the continuum limit.)

The loop model is a modification of those studied in Refs. [37,38], with an additional interaction chosen to drive the model through a transition without explicitly breaking the symmetry between the four short-loop (VBS) states. The model lives on a four-coordinated lattice with cubic symmetry proposed by Cardy [42]. This "3D L lattice" is shown in Fig. 1 (left). Formally, it can be defined by starting with two interpenetrating cubic lattices, C_1 and C_2, with lattice spacing 2, displaced from each other by (1,1,1):

$$C_1 = (2\mathbb{Z})^3, \qquad C_2 = (2\mathbb{Z} + 1)^3. \qquad (2)$$

The faces of C_1 intersect the faces of C_2 along lines: These define the links of the L lattice. The L lattice is bipartite; its two sublattices are marked in yellow and black in Fig. 1.

We orient the links of the L lattice such that each node has two incoming and two outgoing links, with the two incoming links parallel and the two outgoing links parallel, as in Figs. 1 and 2. This assignment is unique up to a reversal of all orientations.

Breaking up each L lattice node by pairing the links in one of the two ways shown in Fig. 2 gives a completely packed loop configuration. In the simplest case, the partition function is just the equal-weight sum over all
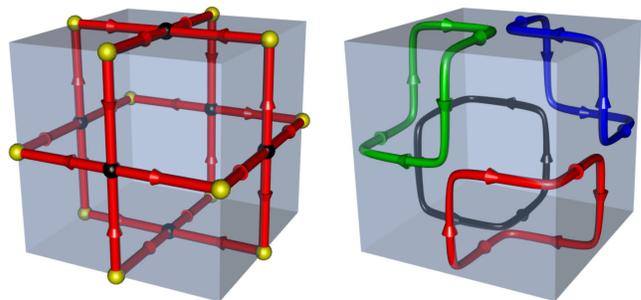

FIG. 1. Structure of L lattice. Left figure: Nodes and links (with associated orientations) in the unit cell of the L lattice. The two sublattices of nodes are indicated. Right figure: One of the four equivalent packings of minimal-length loops on this lattice.
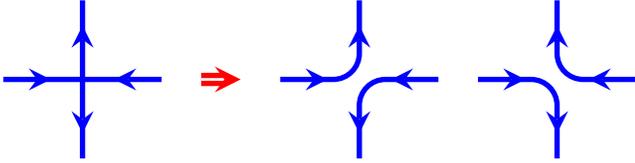
FIG. 2. The two possible configurations of a node ($\sigma_r = \pm 1$).

such configurations, with one of n colors assigned to each loop (the case of main interest here is $n = 2$):

$$Z = \sum_{\substack{\text{colored} \\ \text{loop configs}}} 1. \tag{3}$$

We can, of course, perform the sum over colors explicitly to give $Z = \sum_{\substack{\text{loop} \\ \text{configs}}} n^{\text{no. loops}}$. Note that the loops are automatically consistently oriented since the pairing of links at a node is always between an incoming and an outgoing link.

With the above Boltzmann weight, the system is (for $n \le 4$) in a phase where infinite loops proliferate [37,38]. We wish to add an interaction that drives the system into a phase with only short loops. First, consider the extreme limit of such a phase, which is a configuration in which every loop has the minimal possible length (which is six links). There are only four such configurations, and they are related by lattice symmetry. One is shown in Fig. 1, right.

A general loop configuration is determined by the binary choice of link pairing at each of the nodes. We denote this binary degree of freedom at node r by an Ising-like variable $\sigma_r = \pm 1$. To fix the sign convention for σ, let us pick one of the four minimal-length configurations as a reference and declare that all σ_r are equal to $+1$ in it. The four minimal-length configurations are then those in which all the σs on the same sublattice (A or B) have the same sign. We can define an order parameter of the schematic form $\vec{\varphi} = (\sigma_A, \sigma_B)$ which distinguishes the four short-loop phases. This is the analogue of the VBS order parameter in the quantum problem.

We introduce an interaction between nearest-neighbor σs on the *same* sublattice (i.e., between nodes of like color in Fig. 1):

$$Z = \sum_{\substack{\text{colored} \\ \text{loop configs}}} \exp(-E), \tag{4}$$

$$E = -J\left(\sum_{\langle r,r' \rangle \in A} \sigma_r \sigma_{r'} + \sum_{\langle r,r' \rangle \in B} \sigma_r \sigma_{r'} \right). \tag{5}$$

(The sum over *uncolored* loop configurations is equivalent to a sum over the σs.) With this choice, there is a direct transition at J_c between a phase that has extended loops and $\langle \vec{\varphi} \rangle = 0$, and one that has only short loops and $\langle \vec{\varphi} \rangle \neq 0$.

As we would expect from the quantum correspondence [38], the continuum description of the above model is the

NCCP^{n-1} model. In Sec. V, we show this directly by mapping the loop model to a lattice CP^{n-1} model and coarse graining, paying special attention to the fate of hedgehogs.

III. OVERVIEW OF RESULTS

We first summarize the salient results of our simulations.

At the most basic level, they confirm that the loop model shows the central features of the deconfined Néel-VBS transition and that it probes the same universal physics as the J–Q [5] and related quantum models.

We find a direct and apparently continuous transition between Néel and VBS phases. Figure 3 shows the order parameters for these phases, for various system sizes L, very close to the critical point (see details in Sec. IV A). The data suggest a single transition. This is confirmed by examining finite-size pseudocritical couplings $J_c(L)$ determined from various observables (inset to Fig. 3); all extrapolate to the same value as $L \to \infty$ within error bars, so we are confident that there is a single transition at

$$J_c = 0.088501(3). \tag{6}$$

At small sizes, the estimates of critical exponents are compatible with those found in the J–Q model at similar sizes and in direct simulations of the NCCP^1 model [6,7,9,10,18]. As expected [1,5,7], we see an emergent U(1) symmetry for rotations of the VBS order parameter $\vec{\varphi}$ close to this critical point. [The emergence of this U(1) symmetry is equivalent to the noncompactness of the gauge
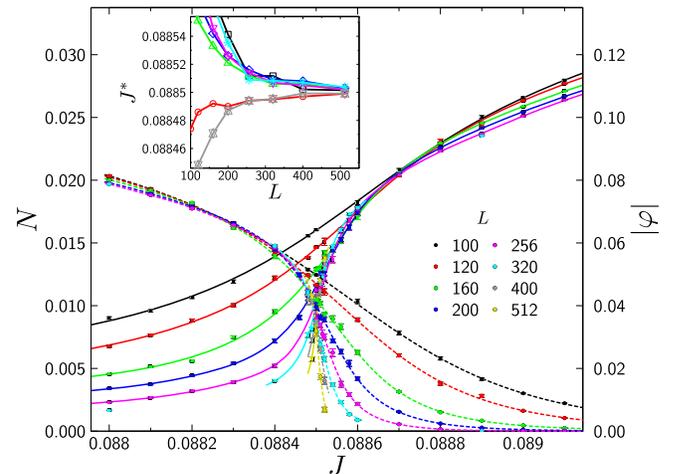

FIG. 3. Néel order parameter N (dashed lines) and VBS order parameter $|\vec{\varphi}|$ (solid lines) as a function of J for several system sizes L. Continuous curves are interpolations using the multiple histogram method [43]. Inset: Pseudocritical couplings $J^*(L)$ obtained from various observables [N (blue rhombi), $|\vec{\varphi}|$ (down-pointing magenta triangles), crossings of $4N$ & $|\vec{\varphi}|$ (grey stars), C (black squares), $\mathcal{N}_s$ (up-pointing green triangles), B_φ (red circles), and V (turquoise asterisks)].
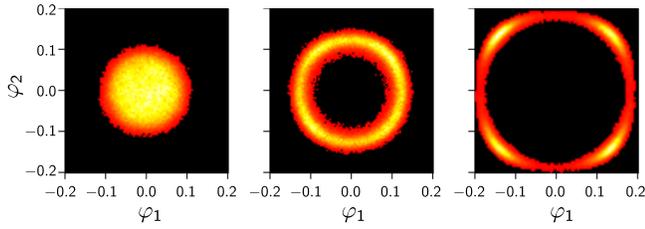
FIG. 4.   Probability distribution of $\vec{\varphi} = (\varphi_1, \varphi_2)$ for size $L = 64$ and (from left to right) $J = 0.0886$, $J = 0.091$, and $J = 0.096$, corresponding, respectively, to the critical point, the VBS phase in the U(1) regime, and the VBS phase in the $\mathbb{Z}_4$ regime. The crossover from U(1) to $\mathbb{Z}_4$ symmetry is analyzed further in Sec. IV B.

FIG. 5.   Spanning number $\mathcal{N}_s$ as a function of J, for various L. Inset: L dependence of critical spanning number $\mathcal{N}_s^*$, defined (1) as $\mathcal{N}_s$ at $J = J_c$ (red dots) and (2) as $\mathcal{N}_s$ at the point where the slope $|d\mathcal{N}_s/dJ|$ is maximal (black dots). Continuous curves are power-law fits, $\mathcal{N}_s^* = AL^p + B$, with exponents $p = 0.61(5)$ and $p = 0.62(3)$, respectively. (Note log-log scale.)

field in the continuum action Eq. (1) [1,2].] Within the VBS phase, the emergent U(1) symmetry survives up to a length scale ξ_{VBS} that is parametrically larger than the correlation length ξ. As for the J–Q model [7], the U(1) symmetry is apparent in the probability distribution for $\vec{\varphi}$; see Fig. 4.

Despite the above features, finite-size scaling properties at the transition are anomalous in various ways. For example, an appropriately defined stiffness for the Néel vector—which would be a universal constant at a conventional critical point—increases slowly with system size, and the critical exponent estimates also drift as the size is increased. Similar features were seen in previous numerical work on the J–Q model [5,9,10,16,17], but the larger sizes considered here show that the scaling violations are stronger than previously apparent. For a detailed picture of the transition, we analyze a variety of observables. Violations of finite-size scaling are visible in almost all quantities and do not decrease as L is increased. For this reason, we are unable to fit the size dependence of the data near the critical point assuming either scaling corrections coming from an irrelevant scaling variable (even if it is very weakly irrelevant) or logarithmic corrections similar to those considered in Refs. [8,9]. (See Secs. 3, IV C, IV E.)

Figure 5 shows the "spanning number" $\mathcal{N}_s$ versus the coupling J for various system sizes. $\mathcal{N}_s$ is the average number of strands which span the system in a given direction, and it is a measure of the stiffness of the Néel order parameter. Instead of tending to a universal value as dictated by standard finite-size scaling, the crossing points $\mathcal{N}_s^*$ drift upwards as a power of L: Fig. 5, inset. (See Sec. IV C for details.)

We calculate the correlation-length exponent ν and the anomalous dimensions $\eta_{\text{Néel}}$ and η_{VBS} using several observables. In the text, results will be presented with statistical errors in the last significant digit shown in brackets in the usual way; for reasons that will be apparent, we are not generally able to estimate systematic errors.

Estimates of ν obtained from finite-size scaling analyses of different quantities are in reasonable agreement but drift significantly, from $\nu \gtrsim 0.6$ at small sizes to values around $\nu \sim 0.46$ for the largest sizes. In contrast, values of ν
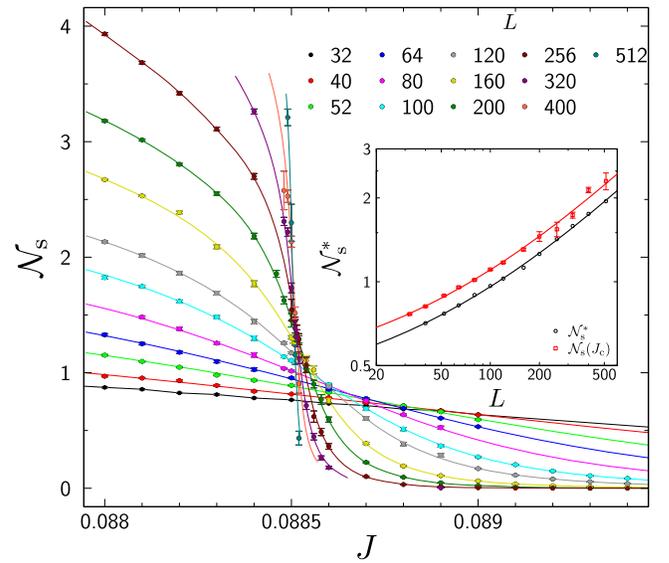
obtained from the variation of the correlation length with distance from the critical point lie in the range 0.45–0.5 with less dependence on size (Sec. IV E).

Strikingly, the behavior of the correlation functions at the critical point suggests different values of the anomalous dimensions $\eta_{\text{Néel}}$ and η_{VBS} depending on the range of r used to extract them. Values obtained from correlation functions at separation $L/2$ both drift from values above 0.2 to values *below* zero at large sizes. Negative ηs *violate* the unitarity bound $\eta \geq 0$ [29,30]. In contrast, there is evidence that behavior for $r \ll L$ is consistent with positive values for the anomalous dimensions. We note that the use of correlators at separation $L/2$ to determine η assumes finite-size scaling, which is a stronger assumption than that of the continuity of the transition, as we discuss in Sec. IV A 1.

In view of the above, the transition can only be continuous if some subtlety invalidates the usual finite-size-scaling expectations. (Of course, in principle, there could be a drastic change in behavior at still larger sizes $L \gg 512$, but the data give no reason to expect this.) Therefore, it is natural to ask whether the transition is first order, with an anomalously large correlation length. But while the probability distributions of various quantities show violations of finite-size scaling, we do not see the standard signs of an incipient first-order transition—double-peaked probability distributions, etc. (Secs. IV A 4, IV C 1, IV D). Figure 6 shows the heat capacity C, which quantifies the fluctuations of the energy. This has a diverging peak at large sizes, as expected for a critical point with a positive heat capacity exponent ($\alpha = 2 - 3\nu > 0$).
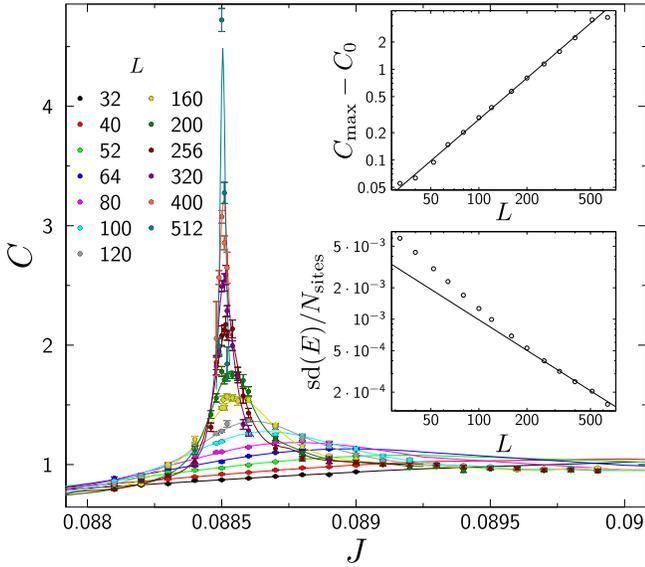
FIG. 6.   Main panel: Heat capacity C versus J. Upper inset: Peak height $C_{\max}$ with constant $C_0 = 0.9836$ subtracted to account for background. The fit is the power law with exponent $\alpha/\nu = 1.52(2)$. Lower inset: Standard deviation in energy at $J = 0.08850$. The fit is with exponent $(\alpha/\nu - 3)/2 = -0.97(4)$.

The peak only emerges from the background at relatively large L. Surprisingly though, the peak fits well to a power law after subtracting a constant to account for the background, $C_{\max} - C_0 \sim AL^{\alpha/\nu}$ (Fig. 6, upper inset). This gives $\nu \simeq 0.44$, corresponding to a divergence $\sim L^{1.52}$. This divergence is much slower than the L^3 expected asymptotically at a first-order transition. For a more intuitive picture, the lower panel of Fig. 6 shows the standard deviation of the energy, divided by the volume, at $J = 0.08850$. For a first-order transition, this should saturate to a constant (proportional to the square of the difference in energy density between the two phases), while here there is no sign of saturation. (More details can be found in Sec. IV D.)

To shed light on these perplexing observations, we analyze the topology of the RG flows in the NCCP^{n-1} theory in Sec. VI. The topology we find allows for a scenario with an anomalously weak first-order transition for a range of n, as a result of a coupling which "walks" (runs slowly) in the proximity of a fixed point located at a spatial dimension slightly below three. This is one possible reconciliation of the above numerical observations.

A more radical possibility is that the transition is continuous but disobeys finite-size scaling because of a dangerously irrelevant variable. This was hypothesized for the SU(3) and SU(4) cases in Ref. [28]. As pointed out below, in this scenario we expect scaling violations in correlation functions when the separation r of the points is comparable with L, but not when r is fixed and $L \to \infty$. In Secs. IV A 1 and VII we consider this possibility in the light of the data.

At present, we cannot rule out either scenario; we sum up the situation in Sec. VII.

IV. NUMERICAL RESULTS

A. Néel and VBS order parameters and correlators

The deconfined transition separates phases that break different symmetries. In the VBS (short-loop) phase, lattice symmetry is broken: This is quantified by the order parameter $\vec{\varphi}$ introduced in Sec. II, whose spatially uniform part is

$$\vec{\varphi} = \frac{\sqrt{2}}{N_{\mathrm{sites}}} \left(\sum_{i \in A} \sigma_i, \sum_{j \in B} \sigma_j \right). \qquad (7)$$

This is normalized so $|\vec{\varphi}|^2 = 1$ for perfect VBS order (there are $N_{\mathrm{sites}}/2$ sites on each sublattice). In the Néel (infinite-loop) phase, SU(2) spin-rotation symmetry is broken. In the loop representation, the magnitude of the Néel order parameter is the probability N that a given link lies on an infinite loop [38]. For a finite system, one may define N to be the probability that a link lies on a strand that spans the system in the z direction. If the transition is second order, we expect finite-size scaling forms [44] for $\vec{\varphi}$ and N,

$$\langle |\vec{\varphi}| \rangle = L^{-(1+\eta_{\mathrm{VBS}})/2} f_{\varphi}(L^{1/\nu} \delta J), \qquad (8)$$

$$N = L^{-(1+\eta_{\mathrm{Néel}})/2} f_N(L^{1/\nu} \delta J), \qquad (9)$$

where $\delta J = J - J_c$. However, attempting a scaling collapse using these forms gives negative ηs and very poor collapse. Raw data for the order parameters were shown above in Fig. 3.

1. Correlation functions

Next, we examine the critical two-point correlation functions for $\vec{\varphi}$ and the Néel vector. In the loop representation, the Néel correlator is simply the probability that two links lie on the same loop [38]. We denote these correlators $G_{\mathrm{VBS}}(r, L)$ and $G_{\mathrm{Néel}}(r, L)$, where r is the separation of the points (taken parallel to a coordinate axis) and L is the system size. Raw data are shown in Fig. 7.

Conventionally, at J_c one would expect

$$G(r, L) = L^{-(1+\eta)} c(r/L), \qquad (10)$$

with different ηs and different scaling functions c for each of the two observables. This would imply a collapse when plotting $L^{1+\eta} G(r, L)$ against r/L. Here, this collapse fails because the effective values of η at small and at large distances differ, as we now quantify.

The full correlation function is relatively complicated because it depends on two length scales, r and L. Therefore, a standard approach is to examine $G_{\mathrm{Néel}}(L/2, L)$ and
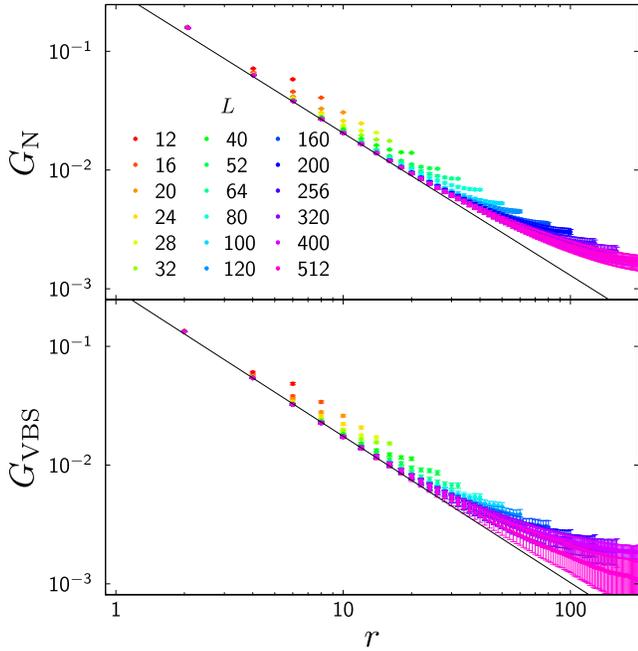
FIG. 7. Correlators $G_{\text{Néel}}(r, L)$ (top panel) and $G_{\text{VBS}}(r, L)$ (bottom panel) plotted against r, for various L. Straight lines correspond to the estimates $\eta_{\text{Néel}} = 0.259(6)$ and $\eta_{\text{VBS}} = 0.25(3)$ from Eq. (12).

FIG. 8. Néel and VBS correlation functions at separation $r = L/2$, plotted against L on a log-log scale. The slopes give effective finite-size exponent values $\eta_{\text{Néel}}(L)$ and $\eta_{\text{VBS}}(L)$, plotted in the left inset. The right inset shows the ratio $G(L/2)/G(L/4)$ versus L.

$G_{\text{VBS}}(L/2, L)$ as a function of L. According to Eq. (10), these scale as $L^{-(1+\eta_{\text{Néel}})}$ and $L^{-(1+\eta_{\text{VBS}})}$, respectively. In Fig. 8 (main panel), we plot these correlators against L on a log-log scale. The gradual change of slope as a function of L indicates a drift in the effective values of $\eta_{\text{Néel}}$ and η_{VBS}. The effective values $\eta_{\text{Néel}}(L)$ and $\eta_{\text{VBS}}(L)$ determined from the slope are shown in Fig. 8 (lower inset). Note that for large L, the estimates for both exponents reach negative values. As mentioned above, negative values of η_{VBS} or $\eta_{\text{Néel}}$ are ruled out for a continuous phase transition governed by a conformally invariant fixed point (though see below).

Another way to quantify the violation of finite-size scaling is via the ratios

$$\frac{G_{\text{VBS}}(L/2, L)}{G_{\text{VBS}}(L/4, L)}, \qquad \frac{G_{\text{Néel}}(L/2, L)}{G_{\text{Néel}}(L/4, L)}, \qquad (11)$$

which should be universal according to Eq. (10) but instead drift significantly with L; see Fig. 8, upper inset.

At certain critical points—for example, in ϕ^4 theory above 4D—a dangerously irrelevant variable invalidates standard finite-size scaling for the correlators. In this scenario, it may happen that the correlator is conventional in the limit $L \to \infty$ [i.e., $G(r, \infty) \sim r^{-1-\eta}$ with $\eta \geq 0$] but anomalous when r is comparable with L, or even with a smaller power of L (see below). Although *a priori* there is no theoretical reason to expect this phenomenon here, it suggests examining correlators in the regime $r \ll L$. From
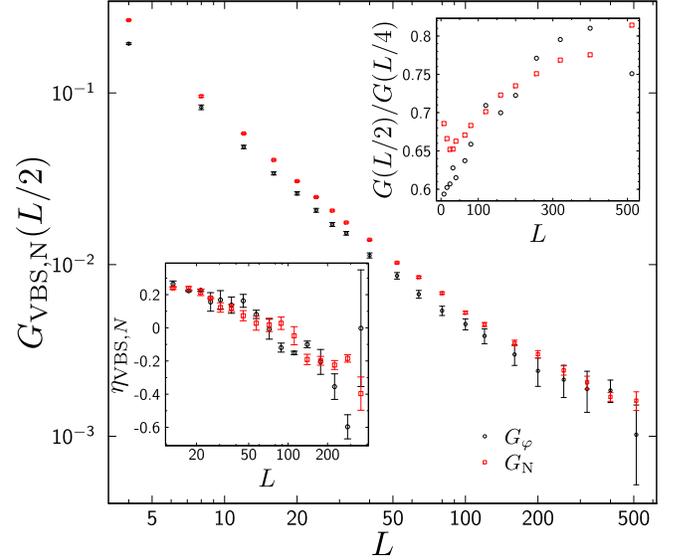
Fig. 7, it is conceivable that a well-defined power law will emerge in the limit $L \to \infty$, although if so, the convergence in L is rather slow.

For further insight, we examine the derivatives of the correlators, $G'_{\text{Néel}}(r) = dG_{\text{Néel}}(r)/dr$ and $G'_{\text{VBS}}(r) = dG_{\text{VBS}}(r)/dr$, in Fig. 9. Remarkably, these quantities show quite clean power-law behavior up to at least $r \sim 100$, with

$$\eta_{\text{Néel}} = 0.259(6), \qquad \eta_{\text{VBS}} = 0.25(3), \qquad (12)$$

and quite good scaling collapse (insets to Fig. 9). Reasonable scaling collapse is also obtained for "subtracted" correlators, defined as $G(r, L) - G(L/2, L)$. Straight lines corresponding to the above exponent values are shown in Fig. 7 for comparison with the raw data.

These results indicate that the strongest effect of the scaling violations is on the zero modes of the fields, which have anomalously large fluctuations. This is suggestive because in ϕ^4 theory above 4D, where the quartic term is dangerously irrelevant, the violation of finite-size scaling is caused by anomalously large fluctuations of the field's zero mode [31]. (Unlike the modes at nonzero momentum, which appear in the kinetic term, the critical fluctuations of the zero mode are controlled only by the irrelevant quartic term.) In that simple theory, we can easily separate out the contribution of the zero mode to the critical correlation function of the scalar field. With periodic boundary conditions, this gives (d is the dimension, and u is proportional to the bare coefficient of the quartic term)

$$\langle \phi(0)\phi(r) \rangle = L^{-(d-2)}c(r/L) + (uL^d)^{-1/2}. \qquad (13)$$
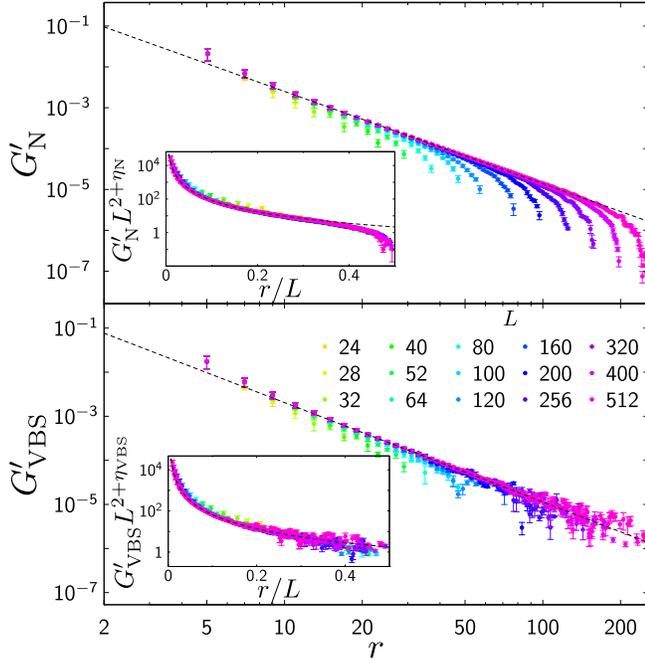
FIG. 9.   Derivatives of Néel and VBS correlators, $dG_{Néel}(r)/dr$ and $dG_{VBS}(r)/dr$. The main panels show raw data and power-law fits (dashed lines) with $\eta_{Néel} = 0.259(6)$ and $\eta_{VBS} = 0.25(3)$. The insets show scaling collapse of $L^{2+\eta}G'$ versus r/L, with the same values for $\eta_{Néel,VBS}$.

The second term, which violates conventional finite-size scaling, dominates as soon as $r \gtrsim L^{d/(2d-4)}$. Since the contribution of this mode to the two-point function depends on L but not on r, scaling can be repaired in this case by differentiation or subtraction.

The fact that this works perfectly in ϕ^4 theory is expected to be a special feature of the fixed point being free (and of the choice of correlator). Nevertheless, the good scaling of $G'_{Néel}$ and G'_{VBS} at the deconfined transition is striking given the strong violation of scaling for the correlators themselves (Fig. 8), and may possibly indicate that a dangerously irrelevant variable is playing a role in the scaling violations. The example of vector $(\vec{\phi}^2)^2$ theory also makes it clear that a dangerously irrelevant variable of this type—associated with controlling anomalously large fluctuations of zero modes—would lead to a spin stiffness that diverges at the critical point instead of taking a universal value [45]. In an appropriate loop gas picture for $(\vec{\phi}^2)^2$ theory, this diverging spin stiffness is associated with the appearance of "anomalously long" loops at the critical point.

2. Fractal structure of loops

The geometrical interpretation of the anomalous dimension $\eta_{Néel}$ is in terms of the fractal dimension of the loops, which according to conventional scaling relations, is given by $d_f = (5 - \eta_{Néel})/2$, and determines the power-law relation between the root-mean-square end-to-end distance

R of a strand and its length (see Ref. [38] for details). This again gives a large positive $\eta_{Néel}$, in contrast to the drift towards negative values seen in the estimate from $G_{Néel}(L/2)$. The simplest fit, taking strands with $R \lesssim 100$ to minimize effects of finite R/L, gives $\eta_{Néel} = 0.42(6)$ (data not shown). We note that this is considerably larger than Eq. (12). However, attempting to include finite R corrections in the fit gives smaller values in the range $0.25 \lesssim \eta_{Néel} \lesssim 0.42$ [47].

3. Susceptibilities

To compare with the estimates above, we calculate $\eta_{Néel}$ and η_{VBS} from the Néel [38] and VBS [48] susceptibilities. These are shown in Fig. 10. According to finite-size scaling, the peaks should diverge as $L^{2-\eta_{Néel,VBS}}$. The insets show log-log plots of the peak heights against L. The slopes indicate a downwards drift from $\eta_{VBS} = 0.164(13)$ to $\eta_{VBS} = -0.35(10)$ and from $\eta_{Néel} = 0.355(9)$ to $\eta_{Néel} = 0.126(3)$.

4. Binder cumulant

Figure 11 shows the Binder cumulant for the VBS order parameter, defined as

$$U_{VBS} \equiv 2 - \frac{\langle |\varphi|^4 \rangle}{\langle |\varphi|^2 \rangle^2}. \tag{14}$$

At a first-order transition, there should be a dip in U_{VBS} which diverges with the system size [49]. In our case, there is no sign of this dip.
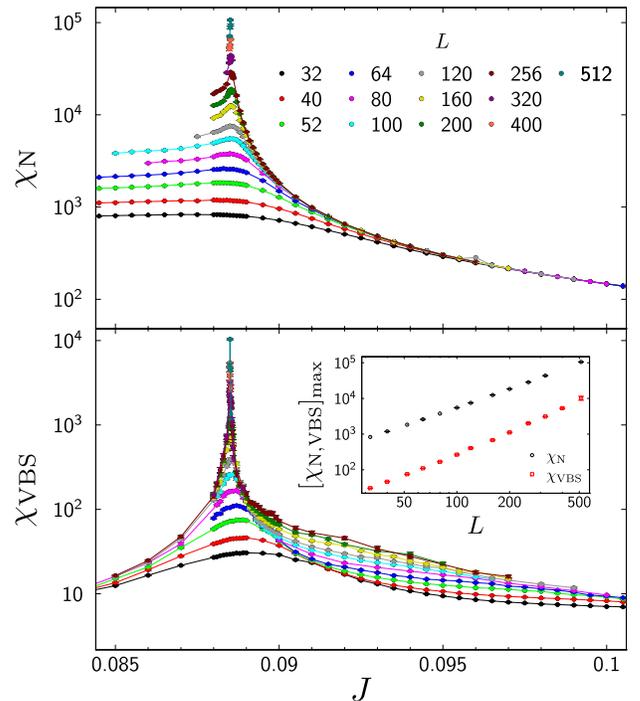

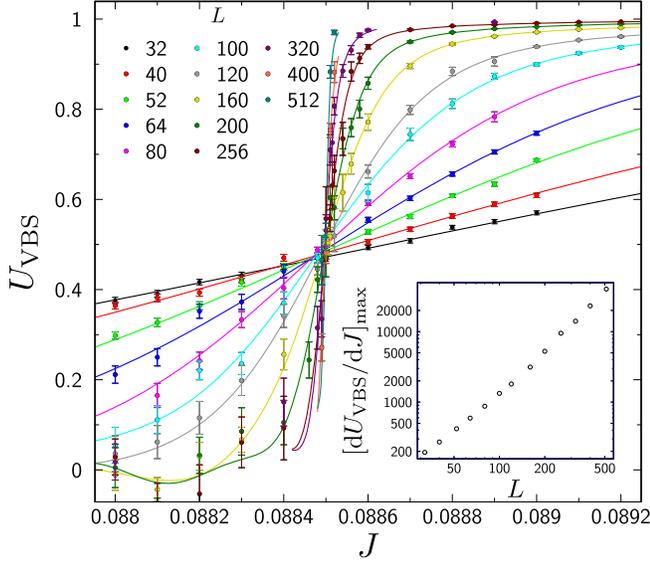FIG. 10.   Susceptibilities for Néel and VBS order parameters. The inset shows peak heights as a function of L.

FIG. 11. U_{VBS} versus J for several system sizes ranging from 32 to 512. Inset: Maximum value of dU_{VBS}/dJ versus L.

FIG. 12. Data for $\langle \cos(4\theta) \rangle$ versus J in several system sizes. Inset: $\langle \cos(4\theta) \rangle$ as a function of the scaling variable $L^{1/\nu_4}(J - J_c)F_2(J - J_c)$.

In the inset to Fig. 11, we plot the maximum value of the slope dU_{VBS}/dJ for each L. For a second-order transition, this value diverges as $L^{1/\nu}$ at the critical point. From the inset, we see that there is different behavior for small and large system sizes, giving $\nu = 0.62(1)$ for sizes $L \leq 64$ and $\nu = 0.476(18)$ for $L \geq 256$. (See Sec. IV E for other estimates of ν.)

B. Emergent symmetries

The deconfined criticality scenario assumes that the leading operator that breaks the symmetry for rotations of $\vec{\varphi}$ from U(1) down to $\mathbb{Z}_4$ is dangerously irrelevant: irrelevant at the critical point but relevant within the VBS phase [2]. This leads to the prediction of a crossover between U(1) and $\mathbb{Z}_4$ symmetry within the VBS phase, on a length scale ξ_{VBS} which is parametrically larger than the correlation length: $\xi_{\text{VBS}} \sim \xi^{1+|y_4|/3}$, where $y_4 < 0$ is the RG eigenvalue of the fourfold anisotropy [50]. This has been confirmed in the J–Q model [7,51].

Figure 4 gave visual evidence for the emergent U(1) symmetry in the loop model. A quantitative measure of $\mathbb{Z}_4$ anisotropy is $\langle \cos 4\theta \rangle$, where $\vec{\varphi} = |\vec{\varphi}|(\cos \theta, \sin \theta)$. Figure 12 shows data for sizes up to $L = 200$. Ignoring scaling violations, the anisotropy should behave as [50]

$$\langle \cos 4\theta \rangle = f(L^{1/\nu_4}\delta J F_2(\delta J)), \quad (15)$$

where $F_2(x) = 1 + ax + bx^2$ takes into account nonlinear dependence of the scaling variable on J (which is needed here because of the larger range of δJ studied for this observable) and $\nu_4 = \nu(1 + |y_4|/3)$. The inset to Fig. 12 shows the attempted scaling collapse using Eq. (15). The exponent $\nu_4 = 1.09(6)$ is obtained from the fit. This
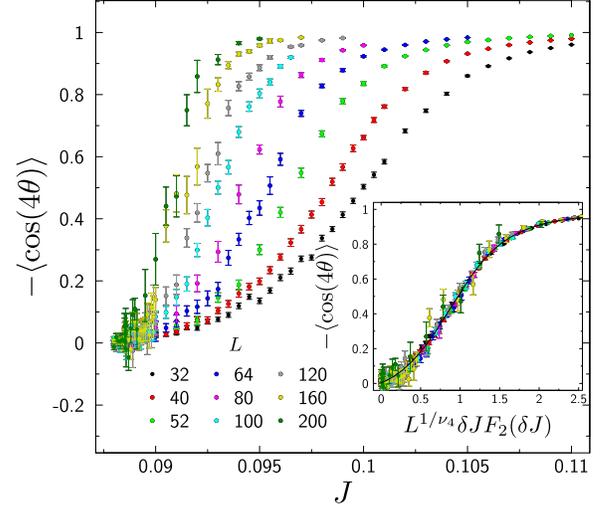
confirms the irrelevance of fourfold anisotropy to the behavior at the transition and to the explanation of the scaling violations. The corresponding value of $|y_4|$ is dependent on the assumed value of ν but is considerably larger than the estimate in Ref. [7] for a variant of the J–Q model.

The closeness of the finite-size effective values of η_{VBS} and $\eta_{\text{Néel}}$ in Fig. 8 and Eq. (12) makes it tempting to speculate about a much larger emergent symmetry—an SO(5) symmetry relating the Néel and VBS vectors. This can be incorporated into an alternative field theory for the deconfined critical point [52,53], which was argued to be equivalent to Eq. (1) [54]. This symmetry enhancement would be analogous to the emergent SO(4) symmetry of the 1D spin-1/2 chain, which relates the spin-Peierls order parameter and the Néel vector [55]. In the future, it would be interesting to check explicitly for SO(5) symmetry. [This has now been addressed in [57].]

C. Néel stiffness and spanning strands

A useful observable is the spanning number $\mathcal{N}_s$, defined as the number of strands that span the system in (say) the z direction. Its mean value $\langle \mathcal{N}_s \rangle$ may be taken as a definition of the stiffness of the Néel order parameter [58]. At a conventional critical point, $\langle \mathcal{N}_s \rangle$ has scaling dimension zero and the scaling form

$$\langle \mathcal{N}_s \rangle = h(L^{1/\nu}\delta J). \quad (16)$$

Therefore, $\langle \mathcal{N}_s \rangle$ should be a universal constant at a critical point, modulo corrections due to irrelevant scaling variables: Plots of $\langle \mathcal{N}_s \rangle$ versus J for different L should cross at J_c. In the VBS phase, $\langle \mathcal{N}_s \rangle$ tends to zero exponentially in L, and in the Néel ordered phase, it grows as L.

The mean spanning number was shown in Fig. 5. Contrary to the above expectation, $\langle \mathcal{N}_s \rangle$ appears to diverge slowly with system size at the critical point. This is manifested in the upwards drift of the crossing points in the main panel. In the inset, we show pseudocritical values $\mathcal{N}_s^*(L)$ defined in two different ways. The data cannot be fitted with conventional scaling corrections from an irrelevant variable, i.e., $\mathcal{N}_s^* = \mathcal{N}_s^{\text{crit}} - AL^y$ with negative y: Attempting such a fit leads to a positive (relevant) y.

Previous work on the SU(2) J–Q model found a drift in a closely related winding number and proposed that this indicated logarithmic corrections to scaling [9]. Similar drifts were found for the SU(3) and SU(4) J–Q models [28], fitting slightly better to a power law than a logarithm. The larger sizes considered here for the SU(2) case show that the divergence is certainly stronger than logarithmic. On attempting to represent it by a pure power law $\mathcal{N}_s^* \sim AL^a$, we find that the exponent drifts upwards, but a power law plus constant

$$\mathcal{N}_s^* \simeq AL^a + B, \qquad a \simeq 0.6 \qquad (17)$$

fits the results for all L. This divergence is of course still slower than the linear behavior expected asymptotically at a first-order transition.

1. Drift of critical probability distribution

In addition to the mean $\langle \mathcal{N}_s \rangle$, we examine the full probability distribution of $\mathcal{N}_s$. Let P_k be the probability that $\mathcal{N}_s$ is equal to $2k$, meaning that k oriented strands span the system in a specified direction and k in the reverse direction. This again has scaling dimension zero, so conventionally we would expect the scaling form

$$P_k = g_k(L^{1/\nu}\delta J). \qquad (18)$$

By contrast, at a first-order transition, where the short-loop and infinite-loop phases coexist, P_k would have a peak at $k = 0$ from the short-loop phase and a peak at $k \propto L$ from the infinite-loop phase.

The distribution P_k obtained numerically is shown in Fig. 13, for various L. To compare different sizes, we tune J for each L so that $P_0 = 0.3$ (using the Ferrenberg method [43]). For comparison, the inset shows the distribution at fixed $J = 0.0885$, very close to the critical point. Contrary to Eq. (18), the data show no sign of tending to a universal distribution. On the other hand, we do not see a double-peaked structure developing either.

The scaling form Eq. (18) would imply that P_k is a universal function of $\langle \mathcal{N}_s \rangle$ for each k. [Explicitly, $P_k = (g_k \circ h^{-1})(\langle \mathcal{N}_s \rangle)$.] Therefore, a plot of, e.g., P_1 against $\langle \mathcal{N}_s \rangle$ would show scaling collapse without the need to adjust any parameters. See Ref. [38] for successful examples of such scaling collapse for the *compact* CP^1 [i.e., $O(3)$] and compact CP^2 models. It is clear from Fig. 13 that
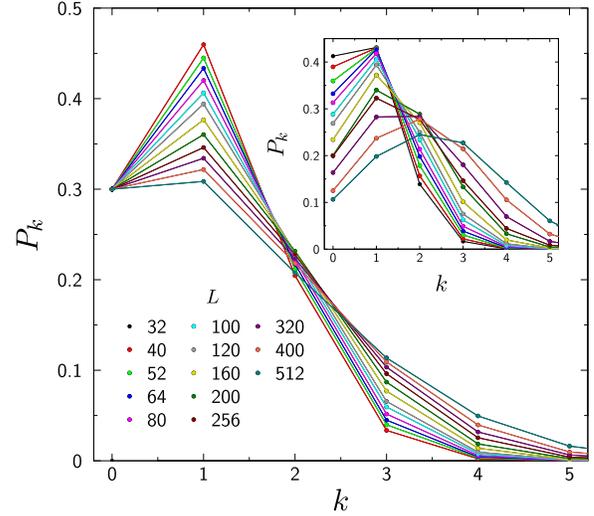

FIG. 13.   Probability P_k that the spanning number $\mathcal{N}_s$ equals $2k$, for a range of L. In the main panel, J is tuned so that $P_0 = 0.3$ for each L. In the inset, J is fixed, $J = 0.08850$.

such a collapse will not work here. Figure 14 shows this for P_1 (interpolating curves are obtained with the Ferrenberg method [43]). The dramatic failure to collapse is quantified in the inset, which shows the maximum value of P_1 as a function of L. At a conventional critical point, this would reach a finite constant as $L \to \infty$, while at a first-order transition, it should tend to zero. There is no evidence for saturation over this size range, though it cannot be ruled out.

We note that the maximum of P_1 decreases below the universal value for the O(3) universality class [38], which is close to 0.4 [a stiffness in the J–Q model also drifts beyond the O(3) value [17]]. This is further confirmation that we are dealing with a direct transition rather than two separate transitions that are too close to be resolved.
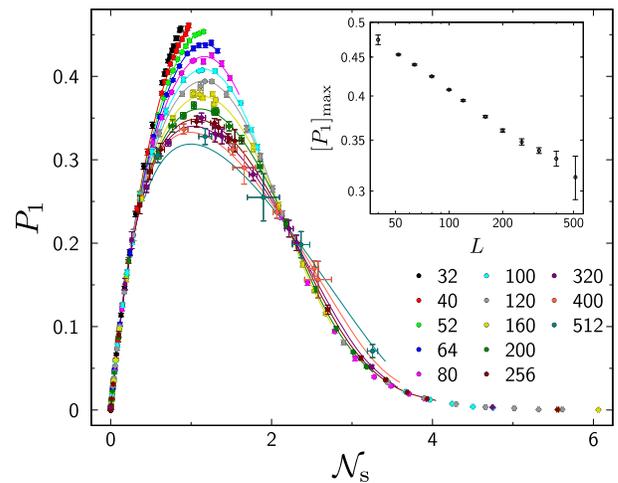

FIG. 14.   Parameter-free scaling: $P_1(J)$ as a function of the average number $\mathcal{N}_s(J)$ of spanning curves. Inset: Size dependence of the maximum of $P_1(J)$ on a double logarithmic scale.
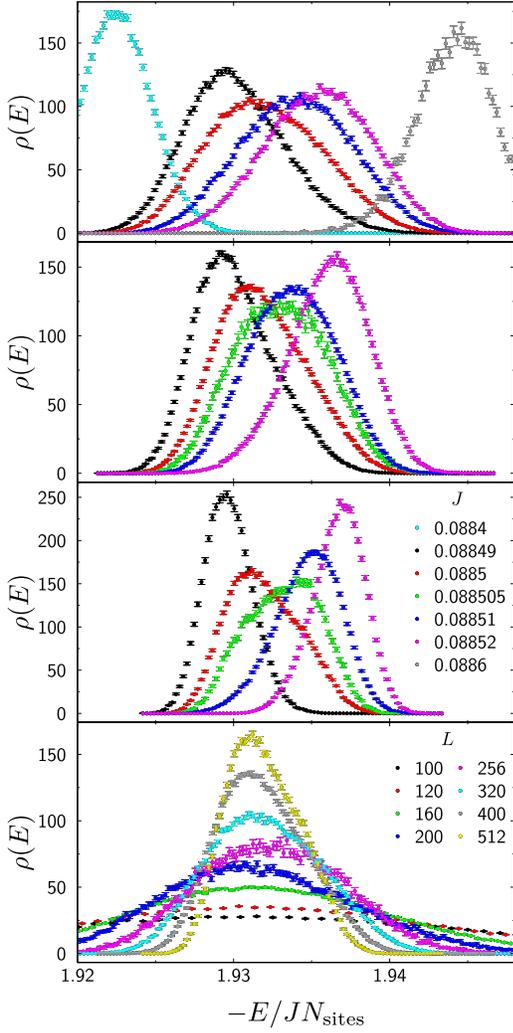
FIG. 16. V_{max} is shown as a function of system size on a double logarithmic scale with the background contribution subtracted. Inset: Raw data for V plotted as a function of J on a semilog-arithmic scale for several values of L.

FIG. 15. First three panels starting from the top: Energy distribution functions for system sizes $L = 320$, 400, and 512, respectively, for various J. Bottom panel: Energy distribution for $J = 0.08850$ for various L.

D. Energy distribution

The behavior of the heat capacity, proportional to the variance in the energy E, has been discussed in connection with Fig. 6. Further information is contained in the full probability distribution for E [which is defined in Eq. (4)]. The top panels of Fig. 15 show how this distribution evolves as J is varied. The bottom panel shows the distribution at $J \simeq J_c$ for various L. We do not see a double-peaked distribution. The width of the critical distribution also decreases with increasing system size, contrary to the expectation for a first-order transition (Fig. 6, lower inset).

The Binder parameter

$$V = \langle E^4 \rangle / \langle E^2 \rangle^2 - 1, \qquad (19)$$

plotted in the inset to Fig. 16, is an alternative quantity for analysis. The data show a peak near the transition, with a
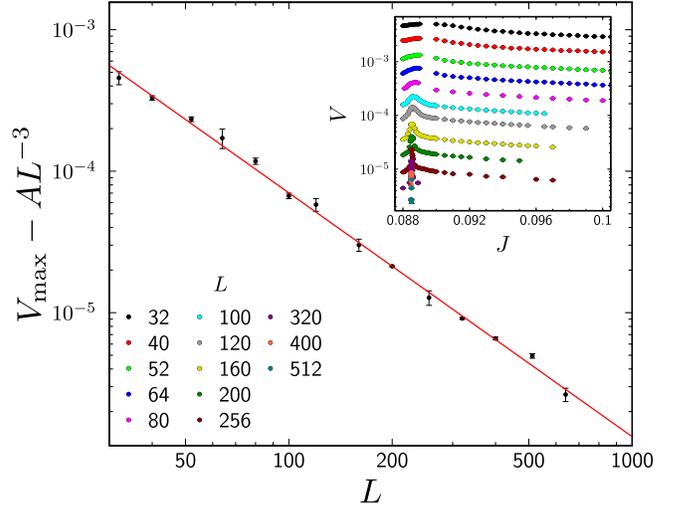
height V_{max} that decreases with L (it is necessary to use the Ferrenberg interpolation method [43] for accurate estimates of V_{max}). At a first-order transition, V_{max} should saturate to a constant as a result of the double-peaked energy distribution, while at a continuous transition with $\alpha > 0$, the peak height should tend to zero as $V_{max} \sim L^{2/\nu - 6}$. Here, a direct estimate of ν using the slope gives a value that drifts from $\nu \sim 0.621(5)$ for system sizes $32 \leq L \leq 64$ to $\nu \sim 0.481(12)$ for $L \geq 256$. However, in addition to the peak, V has a large background contribution scaling as L^{-3} (see inset). It is natural to subtract such a correction. This allows V_{max} to be fitted to the power-law form corresponding to $\nu = 0.468(6)$—see Fig. 16, main panel.

E. Correlation-length exponent

In this section, we discuss two different approaches to determining the correlation-length exponent ν, one relying on finite-size scaling and one not (see Sec. IV A for anomalous dimensions $\eta_{\text{Néel}}$, η_{VBS}).

First, we obtain estimates using the standard finite-size scaling forms for various observables. For example, the Binder cumulant for the VBS order parameter $\vec{\varphi}$ would naively scale as $U_{\text{VBS}} = f_U(L^{1/\nu} \delta J)$, so the maximum value of dU_{VBS}/dJ should grow as $L^{1/\nu}$. Therefore, we can define an effective exponent via $\nu_{\text{eff}}(L)^{-1} = d \log([U'_{\text{VBS}}]_{\text{max}})/d \log L$. We calculate such numerical derivatives using four consecutive system sizes.

Figure 17 shows the resulting estimates $\nu_{\text{eff}}(L)$ from U_{VBS}, from the probability P_0 of having no spanning strands, and the order parameters N and $|\vec{\varphi}|$. $\nu_{\text{eff}}(L)$ drifts from large values, around 0.62 (in accordance with previous studies [5–8,10]) to values around 0.46. The latter is in agreement with the estimate from the heat capacity with
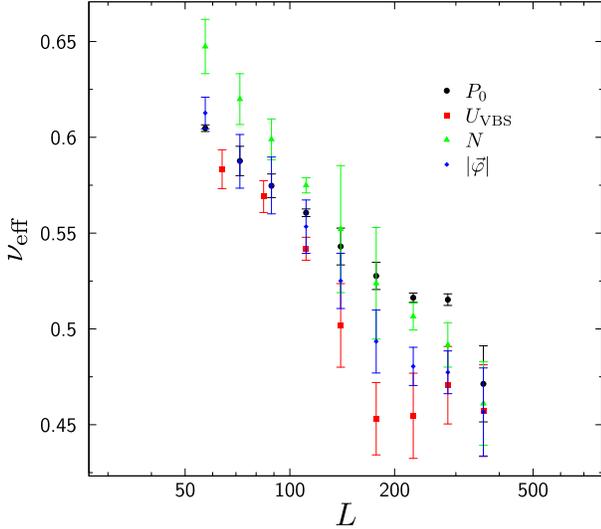
FIG. 17. Size dependence of the effective correlation-length exponent ν_{eff} obtained from finite-size scaling of various quantities.

the background subtracted (Sec. III). Despite the drift, $\nu_{\text{eff}}(L)$ remains above the unitarity bound 2/5. A drift in ν was also identified in Ref. [10].

The above estimates all rely on finite-size scaling forms for observables on the scale of the system size. To avoid the assumption of conventional finite-size scaling, we also estimate ν directly from the correlation length ξ in the regime where $\xi \ll L$. For values of J in the VBS (short-loop) phase, we determine ξ by fitting the L dependence of the spanning number to the expected form
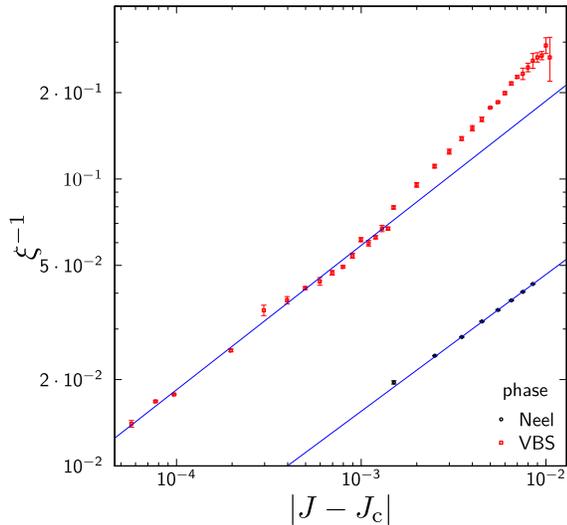

FIG. 18. Estimates of the correlation length obtained from (1) the exponential decay of the spanning number $\mathcal{N}_s$ in the VBS phase, $J > J_c$ (red points) and (2) the coefficient of the linear growth of $\mathcal{N}_s$ in the Néel phase, $J < J_c$ (black points). Note: The overall normalization is arbitrary in the latter case.

$\mathcal{N}_s \propto L^2 e^{-L/\xi(J)}$. In the Néel phase, the spanning number is expected to grow as $\mathcal{N}_s \sim AL/\xi(J)$. This allows us to determine $\xi(J)$ up to the overall constant A.

The results are shown in Fig. 18. The power-law fits shown give $\nu = 0.477(4)$ for the data in the Néel phase and $\nu = 0.503(9)$ for the data in the VBS phase. These values are close to the estimates in Fig. 17 at the largest sizes. But it is remarkable that here this behavior sets in at *much* smaller length scales. For the VBS phase [where we can determine $\xi(J)$ without the complication of an overall constant], the above exponent fits the data well starting from scales as small as $\xi \sim 15$.

We believe that if the transition is indeed continuous, the correlation-length exponent is close to $\nu = 0.5$, thus considerably smaller than most earlier estimates from J–Q and NCCP^1 models. This value is close to $2 + \epsilon$ expansion results for the CP^1 nonlinear sigma model, which should apply to the deconfined critical point, assuming the transition is continuous (see Sec. VI D).

V. FIELD THEORY FOR LOOP MODEL; HEDGEHOG FUGACITIES

Models for completely packed, oriented loops can be mapped to lattice CP^{n-1} models with an unconventional but simple form [37,38]. At first sight, the continuum limit of these models is simply the (compact) CP^{n-1} sigma model. Here, we discuss this continuum limit in more detail and show that hedgehog defects in the CP^{n-1} spin configuration contribute imaginary terms to the action that are analogous to the Berry phases in the Euclidean action for the 2D quantum Heisenberg model [34,35]. These terms are crucial for the present model. By the reasoning of Refs. [1–4], they change the effective continuum description from the compact CP^{n-1} model to NCCP^{n-1}. (By contrast, the imaginary terms were unimportant for the transitions discussed in Refs. [37,38] as a result of the lower lattice symmetry there.)

The quantities of interest are determined by symmetry, so it is enough to consider the case $J = 0$, where the lattice field theory for the loop model is simplest. The CP^{n-1} spins are placed on the links l of the lattice. They are complex vectors $z_l = (z_l^1, \ldots, z_l^n)$, with fixed length $|z|^2 = 1$ and the gauge redundancy $z_l \sim e^{i\varphi_l} z_l$. In a loose notation where the incoming links at a given node are denoted i and i' and the outgoing links o and o', the partition function is

$$Z = \text{Tr} \prod_{\text{nodes}} \left(\frac{1}{2}(z_o^\dagger z_i)(z_{o'}^\dagger z_{i'}) + \frac{1}{2}(z_{o'}^\dagger z_i)(z_o^\dagger z_{i'}) \right). \quad (20)$$

Here, "Tr" is the integral over the zs. Under a gauge transformation of z_l, the terms for the two nodes adjacent to l pick up opposite phases, so the Boltzmann weight is invariant. The mapping between Eq. (20) and the loop

model follows from a straightforward graphical expansion which is described in Ref. [38].

Let us consider the continuum description of Eq. (20). To begin with, take a configuration in which z is slowly varying. Each term in the product over nodes is then close to 1, and we may obtain a continuum sigma-model Lagrangian by a derivative expansion. In 3D, the only term with two derivatives allowed by global, gauge, and lattice symmetries is the standard sigma-model kinetic term. Let us focus on the $n = 2$ case and parameterize CP^1 (which is simply the sphere) using the Néel vector

$$N_a = z^\dagger \sigma_a z, \qquad a = x, y, z, \qquad (21)$$

instead of the gauge-redundant field z. Then,

$$\mathcal{L}_\sigma = \frac{K}{2}(\nabla \vec{N})^2, \qquad (\vec{N}^2 = 1). \qquad (22)$$

A crude way to estimate a bare value of K is to calculate the Boltzmann weight in Eq. (20) for a spin configuration with a uniform twist, giving $K = 1/16$. (For general n, $\mathcal{L}_\sigma$ may be written in terms of the matrix $Q = zz^\dagger - \mathbb{1}/n$.)

The Lagrangian obtained by the derivative expansion can fail to capture the true scaling behavior in two ways. It fails in a trivial way when $\vec{N}$ varies strongly at a node. This will of course be the case in the lattice model, and it leads to an order-one renormalization of the stiffness.

More importantly, the *phase* of z can vary rapidly even if $\vec{N}$ is slowly varying. Nodes where $\vec{N}$ is approximately constant but where this phase varies abruptly contribute imaginary terms to the action. For smooth configurations of trivial topology, these phases cancel. However, in the presence of hedgehog defects, there remain nontrivial phases that are missed by the derivative expansion.

This is because in a configuration with a hedgehog, it is *impossible* to find a gauge in which z is everywhere slowly varying, even far from the hedgehog core. This follows from the fact that topological flux density B_μ, which when integrated over a closed surface gives the signed number of hedgehogs inside, is a total derivative when written in terms of z: $B_\mu = (1/i)\epsilon_{\mu\nu\lambda}\nabla_\mu(z^\dagger\nabla_\nu z)$. If z were continuous, integrating the topological density over a large sphere would give zero. Therefore, z must be discontinuous somewhere on the sphere if the sphere encloses a hedgehog.

A simple calculation is required to determine what effect the imaginary terms have on the weight for a configuration with a hedgehog. We do this calculation in Appendix B. For specificity, we take the hedgehog to be centered on a site of C_1 or a site of C_2—for example, at the center of the cube in Fig. 1. These locations form a body-centred cubic (bcc) lattice, with four sublattices. We find that the weight of a configuration with a hedgehog acquires a fugacity proportional to

$$1, \quad i, -1, \quad \text{or} \quad -i, \qquad (23)$$

depending on which sublattice it sits on. (More precisely, only the relative phase between different locations is meaningful [60].)

This result also generalizes immediately to larger n. The result matches nicely what is found for the 2D quantum Heisenberg model [34–36], where the fugacity for instantons—hedgehogs in spacetime—takes the same set of values as above depending on which of the four sublattices of the square lattice the instanton occurs on.

By symmetry, we infer that the coarse-grained hedgehog fugacity vanishes. In other words, it vanishes as a result of phase cancellation between configurations in which the hedgehog is centered on nearby sites on different sublattices. Thus, the arguments of Refs. [1–4] apply, giving the $NCCP^1$ model [Eq. (1)] as the continuum description.

An alternative argument for the $NCCP^1$ description of square lattice spin-1/2 antiferromagnets was given in Ref. [61], focusing on the VBS order parameter $\vec{\varphi}$ and its vortex defects rather than the Néel order parameter $\vec{N}$ and its hedgehog defects. The key point of this alternative argument is that a vortex in the VBS order parameter carries a single unpaired spin at its center. In spacetime, this corresponds to an extended spinon worldline running along the vortex core. This has a direct interpretation in the loop model: A vortex line in the node order parameter $\vec{\varphi}$ has a single extended loop running along its core. We have confirmed this explicitly by constructing such configurations.

In previous work, we have considered transitions in a different version of the loop model which does *not* preserve the full lattice symmetry [37,38]. The transitions in that less-symmetric model are described by the *compact* CP^{n-1} model, unlike the present loop model whose transition is described by $NCCP^{n-1}$. This is because breaking lattice symmetry spoils the cancellation between the values in Eq. (23), leaving a nonzero hedgehog fugacity. This result allows the standard critical behavior of the compact CP^{n-1} model [i.e., of the usual O(3) model when $n = 2$]. We note that in the case $n = 3$, the *compact* CP^2 model appears to show an interesting continuous transition that is naively forbidden by Landau theory [37,38,62]. A RG explanation for why the expectation from Landau theory breaks down in this case was given in Ref. [38].

VI. RG FLOWS IN THE $NCCP^{n-1}$ MODEL (n–COMPONENT ABELIAN HIGGS MODEL)

In this section, we make a conjecture for the topology of the RG flows in the $NCCP^{n-1}$ model, the n-component generalization of Eq. (1) with $z = (z_1, ..., z_n)$:

$$\mathcal{L} = |(\nabla - iA)z|^2 + \kappa(\nabla \times A)^2 + \mu|z|^2 + \lambda|z|^4. \qquad (24)$$

This generalization is also known as the n-component Abelian Higgs model. We treat both n and the spatial dimension d (between 2 and 4) as continuously varying.

Scaling violations are seen in a wide variety of different lattice models that are related to this field theory (at $n = 2$) and persist to very large length scales [63,64], so we believe a plausible explanation for them should appeal to universal physics of the NCCP^{n-1} model and not to accidental features of specific Hamiltonians. Results for SU(3)- and SU(4)-symmetric models ($n = 3, 4$ [10,28]) suggest that a satisfactory explanation should also account for scaling violations across a range of n.

Figure 19 shows the basic topology of the RG flows we find. This is a sheet of RG fixed points projected on the space of n, d, and a scaling variable λ. [Close to 4D, λ is the quartic coupling in Eq. (1), but in lower dimensions, one cannot make this identification.] The RG flow is parallel or antiparallel to the λ axis since n and d do not flow. λ is irrelevant on the critical sheet and relevant on the tricritical sheet. The strongly relevant coupling that drives the transition (i.e., the mass) is not shown since we consider the theory at the critical value. For any fixed value of n between zero and $n_{*4} \simeq 183$, the critical point exists so long as we are sufficiently close to two dimensions. When d is increased, the critical point disappears at a universal value $d_*(n)$, by merging with the tricritical point.

To begin with, consider three limits in which the NCCP^{n-1} model is solvable. First, it is tractable by saddle-point at large n, where it yields a nontrivial critical point for $2 < d < 4$. This critical point describes a direct transition between a Higgs phase, where z is condensed and SU(n) symmetry is broken, and a Coulomb phase where SU(n) symmetry is unbroken and the gauge field A is massless.
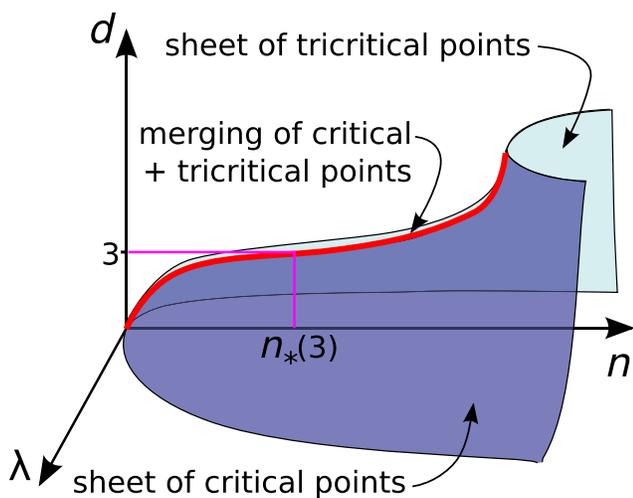

FIG. 19.   Topology of the sheet of RG fixed points for dimensionalities around three (the limiting cases $d = 2$ and $d = 4$ are not shown).

The field theory is also tractable in a $4 - \epsilon$ expansion [65]. For infinitesimal ϵ, a weak-coupling critical point exists only if n is greater than or equal to a value that we denote n_{*4}. This value is quite large, $n_{*4} \simeq 183$. In fact, in the regime $n > n_{*4}$ where the critical point exists, the $4 - \epsilon$ expansion also yields a *tricritical* point at a smaller value of the quartic coupling λ. As n approaches n_{*4} from above, these two fixed points approach each other, and they annihilate when n reaches n_{*4}. For $n < n_{*4}$, there is no nontrivial fixed point: The theory is expected to flow to a discontinuity fixed point at large negative λ representing a first-order transition.

Finally, the NCCP^{n-1} model can be studied in $2 + \epsilon$ dimensions by switching from a soft-spin formulation to a nonlinear sigma model [66–68]. In this regime, a continuous phase transition is found for all values of n greater than zero. (The "replicalike" regime $n \leq 1$ is meaningful and describes certain classical loop models [37,59,69].) In the $2 + \epsilon$ approach, it does not matter whether the nonlinear sigma model is formulated with a dynamical U(1) gauge field or as a pure nonlinear sigma model with target space CP^{n-1}: The two formulations give identical results [66]. (When the dynamical gauge field is included, its coupling flows to infinity, so it can be integrated out, leaving the usual CP^{n-1} nonlinear sigma model.)

A crucial point, made in Ref. [32], is that the fixed point found in the large n approach is the *same* as that found in both the $2 + \epsilon$ and $4 - \epsilon$ expansions. This can be seen by comparing the results for the critical exponents in the regions of overlap of the expansions. Viewing n and d as continuous variables, there is therefore a continuous family of fixed points in a region of the (n, d) plane for $2 < d < 4$ and sufficiently large n [32]. This region is defined by $n > n_*(d)$, where $n_*(d)$ is the d-dependent value of n at which the fixed point disappears. From the $4 - \epsilon$ approach, we know that the limiting behavior as $d \to 4$ is $n_*(d) \to n_{*4} \simeq 183$ [70], and from the $2 + \epsilon$ expansion, we know that $n_*(d) \to 0$ as $d \to 2$. Using the sigma model, we may also argue that the slope of $n_*(d)$ is finite as $d \to 2$ (see the endnote [72]). The value of $n_*(3)$ is not known, but it is possible to show that $n_*(3) > 1$ (Sec. VI C). We assume that $n_*(d)$ increases monotonically with d.

We can go further by noting that in the $4 - \epsilon$ expansion, the way in which the nontrivial fixed point disappears at $n_*(d)$ is by annihilation with a tricritical point. On the basis of continuity, we expect that the mechanism for the disappearance of the fixed point at $n_*(d)$ is the same for all d. This leads directly to the topology in Fig. 19. It will be convenient to denote the value of d where the merging of the critical and tricritical points happens, for a given n, by $d_*(n)$.

A. RG flows close to the merging line

Since $n_{*4} \simeq 183$ is relatively large, the average slope of the line $d = d_*(n)$ is small. It is therefore possible that there

is a broad range of n values where the line lies close to three dimensions, i.e., where $|d_*(n) - 3|$ is small. So it is worth studying the RG flows in this regime.

On the line, λ is marginal. After rescaling and shifting λ by a constant, its RG equation is

$$\frac{d\lambda}{d \ln L} \simeq -\lambda^2. \tag{25}$$

Moving slightly away from the line, the RG equation becomes, to lowest order in $d_*(n) - d$,

$$\frac{d\lambda}{d \ln L} \simeq a(n)(d_*(n) - d) - \lambda^2 \tag{26}$$

with an unknown but universal positive constant $a(n)$. This equation encapsulates the fact that when $d > d_*(n)$, there is no fixed point, and when $d < d_*(n)$, both a critical point and a tricritical point exist, at $\lambda = \pm\sqrt{a(n)(d_*(n) - d)}$.

Now fixing on $d = 3$, we define the universal quantity $\Delta(n) = a(n)(d_*(n) - 3)$, which is zero at $n = n_*(3)$ (where the critical point disappears in 3D) and small over the range of n where the merging line lies close to $d = 3$:

$$\frac{d\lambda}{d \ln L} \simeq \Delta(n) - \lambda^2. \tag{27}$$

When $n < n_*(3)$, $\Delta(n)$ is negative and there is no fixed point in 3D. Instead, the RG flows go to large negative λ, suggesting a first-order transition. However, if we are close to the line, so $|\Delta(n)|$ is small, the RG flow becomes very slow. Integrating Eq. (27) shows that this implies an exponentially large correlation length at this transition:

$$\xi \sim \exp\left(\pi/\sqrt{|\Delta(n)|}\right) \tag{28}$$

with a nonuniversal prefactor. (A similar phenomenon occurs in the 2D Q-state Potts model for $Q \gtrsim 4$ [74].)

For $n > n_*(3)$, there *is* a conventional critical point at $\lambda = \sqrt{\Delta(n)}$. But if we are close to the line, the leading irrelevant RG eigenvalue y_{irr} at this critical point is small, implying large corrections to scaling: From Eq. (26),

$$y_{irr} \simeq -2\sqrt{\Delta(n)}. \tag{29}$$

B. Interpretation

At first sight, the topology we have found for the RG flows suggests two possible explanations for the scaling violations.

First, if we (speculatively) assume that $n_*(3) > 4$, but that the merging line lies close to $d = 3$ over the range $2 \leq n \leq 4$, then we obtain an anomalously weak first-order transition for $n = 2, 3, 4$. In this scenario, there is pseudocritical behavior (with drifting exponents [75]) up to the exponentially large length scale of Eq. (28), thanks to the "nearby" fixed point at slightly smaller spatial dimension. The virtues of this scenario are that it appeals to universal

features of the RG flow and so may explain why numerous different lattice models see very similar scaling violations, and that it can produce scaling violations over a range of n.

(Note that if $|\Delta|$ is very small, there exists a range of sizes where λ appears to be a conventional marginally irrelevant variable. However, this range ends at a size L_* which is parametrically smaller than ξ [76] when ξ is large. The basic point is that the stages of the RG flow with $\lambda > 0$ and with $\lambda < 0$ take roughly equal amounts of RG time, but the latter corresponds to a vastly larger length scale because of the logarithmic relationship between length and RG time.)

Second, we might try to explain the scaling violations differently by postulating that in 3D the values $n = 2, 3, 4$ lie just below the merging line [$n_*(3) < 2$] so that $\Delta(n)$ is small and positive for $n = 2, 3, 4$. This would give a true critical point with large (but conventional) scaling corrections due to a small irrelevant exponent y_{irr}. However, our numerical results strongly indicate that a small y_{irr} is not sufficient, on its own, to explain what we see.

We emphasize that since our argument fixes the topology of the RG flows but not the numerical value of $n_*(d)$, the scenario above for a weak first-order transition is speculative. In Sec. VII, we discuss another possible conjecture.

C. Bound on $n_*(3)$

The value of $n_*(3)$ is not known, but we can argue that

$$n_*(3) > 1. \tag{30}$$

This may look surprising at first glance since the single-component Abelian Higgs model, $n = 1$, certainly has a continuous phase transition in 3D. This transition is related by duality to that of the XY model [77]. Equation (30) means that this "inverted XY" phase transition does not lie on the sheet we are considering: It is not analytically connected to the deconfined critical point at large n [78].

Formally, one can see this as follows. If the inverted XY transition did lie on the critical sheet of Fig. 19, we could describe it by setting $n = 1$ in the $2 + \epsilon$ expansion of the CP^{n-1} nonlinear sigma model. But this is evidently not the case. The inverted XY transition is a conventional thermodynamic phase transition with nontrivial signatures in the free energy. In contrast, the sigma model at $n = 1$ is a replicalike theory, in which the number of degrees of freedom becomes zero and the free energy vanishes identically. The same reasoning implies that $n_*(3)$ is strictly greater than 1. Otherwise, the $n = 1$ model would have a Higgs transition with an unphysical replicalike continuum description.

Instead of being connected to the critical points in Fig. 19, the inverted XY transition is the $n = 1$ limit of a much simpler transition—namely, that which (for $n > 1$) separates the Higgs phase, where z is condensed, from a *pair* condensed phase where the bilinear $zz^\dagger$ is condensed but z itself is not. (This phase appears for appropriate couplings [19,79].) SU(n) symmetry is broken on *both* sides of this transition, so it is not like the critical points in

Fig. 19. One can check that the transition is in the inverted *XY* universality class for all *n* [as the interactions between the critical sector and the Goldstone modes of the broken SU(*n*) symmetry are irrelevant], so the *n* dependence of the critical behavior is trivial [80].

D. "Failure" of the 2+ε expansion of the O(3) model

The CP^1 nonlinear sigma model is the O(3) nonlinear sigma model by another name, as the target space is the sphere (CP^1 = S^2). Therefore, the topology of the flows in Fig. 19 confirms that the standard $2 + \epsilon$ expansion of the O(3) sigma model does *not* describe the Wilson Fisher critical point of the 3D O(3) model. Instead, setting $\epsilon = 1$ in this expansion describes the SU(2) deconfined critical point, if it exists [or nothing at all if the critical point vanishes at a $d_*(2)$ below 3]. The applicability of the $2 + \epsilon$ expansion to the Abelian Higgs model was also argued in Ref. [32].

Although this is contrary to what is often assumed, it should not be surprising in the light of knowledge about hedgehogs in the 3D O(3) model [4,81]. Suppressing these topological defects has been convincingly argued to change the critical behavior [4]. It is natural that the $2 + \epsilon$ expansion, which considers only spin waves, describes the behavior in the absence of hedgehogs [82].

The conclusion is also supported by a RG approach to the O(*M*) model that employs a double expansion in $(d - 2)$ and $(M - 2)$ [33]. This shows that the standard $2 + \epsilon$ expansion fails to capture the critical behavior of the O(*M*) model when *M* is smaller than a *d*-dependent critical value M_c. To first order in $d - 2$, the relationship is $(M_c - 2) \simeq (\pi^2/4)(d - 2)$, which gives $M_c \sim 4.5$ in 3D. While higher-order corrections in $(d - 2)$ could be significant, this result suggests $M_c > 3$ [33].

Reference [33] also notes the poor agreement between the $2 + \epsilon$ exponents in 3D and the exponents of the O(3) model in 3D. For example, ν is equal to $\nu = 1/2$ at order ϵ^2, or to 2/5 at order ϵ^3 [67,84]. In the light of the preceding, we should instead apply these exponents to the SU(2) deconfined transition. Indeed, the ϵ-expansion values $\nu = 1/2$ and $\nu = 2/5$ are remarkably close to our best estimates of ν (see Sec. IV E).

VII. INTERPRETATION AND CONCLUSIONS

We have argued that the scaling violations at the deconfined critical point are too severe to be explained as corrections to scaling from a weakly or marginally irrelevant scaling variable. This clearly excludes the most conventional scenario for the first time. We have also sharpened the possible alternatives as follows.

Some of our numerical results suggest that estimates of the exponents ν, $\eta_{\text{Néel}}$, and η_{VBS} may be better defined if we avoid using finite-size scaling to obtain them (see, in particular, Secs. IV A 1 and IV E)—although, of course, abandoning finite-size scaling restricts us to length scales

much smaller than the system size. The most radical conjecture would therefore be to attribute the scaling violations to a dangerously irrelevant variable (DIV) which leaves critical behavior intact but modifies finite-size scaling (see also Ref. [28]). In the simplest picture, the role of this DIV would be to cut off fluctuations of some zero mode(s) of the fields that are unbounded in the pure fixed-point theory. The main examples we know of this phenomenon are in free theories (such as ϕ^4 theory above 4D [31] or the quantum Lifshitz theory [85]); another type of example is in theories that are dual to free theories (see endnote [86]). Further work is required to determine whether it is a plausible possibility in an interacting theory like Eq. (1).

The alternative possibility of an anomalously weak first-order transition has been discussed in detail in Sec. VI. We have shown that, in principle, there is a mechanism by which a very large correlation length can appear without the need for fine-tuning of the Hamiltonian and that in this scenario there would be pseudocritical behavior over a large range of scales, with (for example) drifting critical exponents. Such a possibility is hard to exclude numerically. We note, however, that we do not see the usual signs of an incipient first-order transition, despite studying much larger scales than the early simulations used to argue for first-order behavior in the J–Q model [16]. The first-order scenario would also leave the good scaling of, for example, the derivatives of the correlators (Sec. IV A 1) a mystery.

Intriguing questions therefore remain for the future. The loop model is an ideal platform for further work on the deconfined transition, since it provides an intuitive geometrical picture and since isotropy in three dimensions is a convenient feature. It would also be interesting to perform simulations at other values of *n* [which in the formulation just after Eq. (3) need not be an integer] in order to probe the scenario of Sec. VI.

Various modifications to the loop model are possible. For example, one may allow a third node configuration (see Fig. 2) in which the two incoming links are joined and the two outgoing links are joined, so that the loops are no longer consistently oriented. The symmetry is then broken from SU(*n*) to SO(*n*), and the relevant field theories are RP^{n-1} models [37,38,46,59] which can show a $\mathbb{Z}_2$ spin liquid phase [87,88]. One may also study the effects of various anisotropies and symmetry-breaking perturbations. Finally, the loop model generalizes to four dimensions, where it may be a useful tool to search for new types of critical behavior arising in $3 + 1$D quantum magnets.

APPENDIX A: METHODS

The numerical procedure is as follows. An initial state is constructed by choosing at random one of the two possible configurations of a node with equal probabilities. Loops are then formed by following turning instructions at each node. We generate the fugacity n from a sum over loop colors, assuming n is an integer. So a color is associated with each loop chosen with equal probability from n alternatives.

Subsequent states are generated using three kinds of parallelized Monte Carlo moves to ensure that at equilibrium configurations are distributed according to the partition function, Eq. (4). The first one updates the state of the nodes using a checkerboardlike algorithm. Each node, if its four links have the same color, changes its state with probability $\min\{\exp[-2J\sigma(i)\sum_{j_{nn}}\sigma(j)],1\}$. The updates of all the nodes in the lattice are done in three stages. In the L lattice, there are two sublattices A and B. Each sublattice is tripartite, and the three sublattices are simple cubic types. At each time, one sublattice of A and one sublattice of B are updated. The second type of Monte Carlo move chooses a link at random and changes the color of all the links of the associated loop to a different color, chosen with uniform probability from the $n-1$ possibilities. This move is also parallelized by letting each thread choose a link and change the color of the loop if it is not already visited. The third type of move is to recolor all loops in the system, with the new colors selected independently and at random for each loop. It is designed to ensure that the colors of short loops equilibrate efficiently.

A number of these moves are combined to form a composite update which we term a Monte Carlo sweep. The ingredients in a single sweep are as follows. First, we iterate 20 times a sequence in which moves of the first two types are intercalated and repeated for each of the three sublattices. Then, we apply the third type of move. Measurements are performed once every Monte Carlo sweep. The autocorrelation function of the energy is used to estimate a correlation time. The blocking and bootstrap methods [89] are used to estimate errors.

As an interpolation scheme, we have used Ferrenberg's multiple histogram method [43] to obtain a continuous set of values as a function of J of the different quantities. This method is also employed whenever a derivative has to be calculated and a maximum or minimum has to be obtained. Errors related to this technique are calculated using the bootstrap method.

We consider system sizes of up to 3.9×10^8 links or lateral size $L = 640$, with extensive results for $L \leq 512$. The minimum number of Monte Carlo sweeps used is 10^5 for any J and L, and it increases with decreasing L.

APPENDIX B: CALCULATION OF HEDGEHOG FUGACITY

Regarded as a lattice magnet for classical CP^{n-1} spins, the partition function (20) has the peculiar feature that although it is both local and gauge invariant, it is not simply expressed in terms of the gauge-invariant quantity $\vec{N}$ (for $n = 2$) or Q (for larger n). The consequence of this, as noted in Sec. V, is that the sigma-model action arising from a derivative expansion may need to be supplemented by purely imaginary terms from nodes at which the phase of z changes abruptly. In the presence of hedgehogs, such nodes are inevitable, even far from the hedgehog core. As a result, the hedgehog fugacity acquires a spatially varying phase.

For simplicity, we take the hedgehogs to sit at the center of a cube of C_1 or C_2 [Eq. (2)], for example, at the center of the cube in Fig. 1 (left). These locations form a bcc lattice. We take the origin at one such bcc site and the coordinate axes parallel to the links.

Focusing on the case $n = 2$ (the generalization to larger n is immediate), let us first consider the representative configuration in which the hedgehog is centered at the origin and the Néel vector $\vec{N}$ (defined in Sec. V) points in the radial direction. In polar coordinates, $0 \leq \theta \leq \pi$, $0 \leq \varphi < 2\pi$, this is

$$\vec{N} = (\sin\theta\cos\varphi, \sin\theta\sin\varphi, \cos\theta), \quad (B1)$$

where the coordinates of a link are those of its midpoint. To write this in terms of $\vec{z}$, we must pick a gauge. It is convenient to choose one in which the Boltzmann weight

$$e^{-S_{\text{node}}} = \frac{1}{2}[(z_o^\dagger z_i)(z_{o'}^\dagger z_{i'}) + (z_o^\dagger z_{i'})(z_{o'}^\dagger z_i)] \quad (B2)$$

is approximately equal to 1 for as many nodes as possible. For the links with positive and negative z coordinates ($\theta < \pi/2$ and $\theta > \pi/2$), we take, respectively,

$$z = (\cos\theta/2, e^{i\varphi}\sin\theta/2), \quad z = (e^{-i\varphi}\cos\theta/2, \sin\theta/2). \quad (B3)$$

We see from Fig. 1 that there are also links in the equatorial plane. For these links, we take

$$z = \frac{1}{\sqrt{2}}(e^{-i\varphi/2}, e^{i\varphi/2}). \quad (B4)$$

Now consider $e^{-S_{\text{node}}}$. In fact, it will suffice to consider only nodes far from the core and to treat z as constant except for the discontinuities in our gauge choice: Other contributions to the action are either included in the spatially *independent* amplitude of the hedgehog fugacity or are already captured by the naive derivative expansion.

With the above gauge choice, the nodes at which z varies abruptly all lie in the equatorial plane and have two of their

links within this plane, one above it and one below. Figure 1 shows four such nodes (all black). From Eqs. (B2)–(B4), we find that most of these nodes have $e^{-S_{\text{node}}} \simeq 1$, despite the variation in the phase of z. However, there is a string of nodes along the positive x axis ($\varphi = 0$, $\theta = \pi/2$), each of which contributes a minus sign to the Boltzmann weight (i.e., $e^{-S_{\text{node}}} \simeq -1$ for these nodes). If we translate the core of the hedgehog by the vector (2, 0, 0), while keeping the configuration far from the core fixed, we change the number of nodes on this string by 1. Therefore this translation changes the sign of the Boltzmann weight.

Let the phase term in the hedgehog fugacity be denoted

$$\exp(i\eta(r)), \qquad (\text{B5})$$

where the spatial vector r lies on a bcc site. [An "antihedgehog" of negative topological charge has phase factor $e^{-i\eta(r)}$, as we see from Eq. (B2) and the fact that complex conjugating z exchanges hedgehogs and antihedgehogs.] The phase $\eta(r)$ is defined only up to a constant: For example, in a closed system with periodic boundary conditions, there are equal numbers of hedgehogs and antihedgehogs, so the constant part of η drops out.

It may be seen from Fig. 1 that the translational symmetry between bcc sites is not spoiled by the link orientations. Using this, we may argue that $\eta(r)$ is of the form $\eta(r) = k.r$ for some momentum k. By the above calculation, $e^{i\eta(r)} = -e^{i\eta(r+2\hat{x})}$, where $\hat{x} = (1, 0, 0)$. By symmetry, we have similar results for translations in the y and z directions. This is enough to fix k up to a sign:

$$k = \pm \frac{\pi}{2}(1, 1, 1). \qquad (\text{B6})$$

One of these signs applies to the hedgehog and one to the antihedgehog. We have not fixed which is which, but it does not matter.

With this k, the hedgehog fugacity takes four distinct values on the four sublattices of the bcc lattice, proportional to ± 1 and $\pm i$. This is the result quoted in Sec. V.

---

[1] T. Senthil, A. Vishwanath, L. Balents, S. Sachdev, and M. P. A. Fisher, *Deconfined Quantum Critical Points*, Science **303**, 1490 (2004).

[2] T. Senthil, L. Balents, S. Sachdev, A. Vishwanath, and M. P. A. Fisher, *Quantum Criticality beyond the Landau-Ginzburg-Wilson Paradigm*, Phys. Rev. B **70**, 144407 (2004).

[3] T. Senthil, L. Balents, S. Sachdev, A. Vishwanath, and M. P. A. Fisher, *Deconfined Criticality Critically Defined*, J. Phys. Soc. Jpn. **74**, 1 (2005).

[4] O. I. Motrunich and A. Vishwanath, *Emergent Photons and Transitions in the O(3) Sigma Model with Hedgehog Suppression*, Phys. Rev. B **70**, 075104 (2004).

[5] A. W. Sandvik, *Evidence for Deconfined Quantum Criticality in a Two-Dimensional Heisenberg Model with Four-Spin Interactions*, Phys. Rev. Lett. **98**, 227202 (2007).

[6] R. G. Melko and R. K. Kaul, *Scaling in the Fan of an Unconventional Quantum Critical Point*, Phys. Rev. Lett. **100**, 017203 (2008).

[7] J. Lou, A. Sandvik, and N. Kawashima, *Antiferromagnetic to Valence-Bond-Solid Transitions in Two-Dimensional SU(N) Heisenberg Models with Multispin Interactions*, Phys. Rev. B **80**, 180414 (2009).

[8] A. Banerjee, K. Damle, and F. Alet, *Impurity Spin Texture at a Deconfined Quantum Critical Point*, Phys. Rev. B **82**, 155139 (2010).

[9] A. W. Sandvik, *Continuous Quantum Phase Transition between an Antiferromagnet and a Valence-Bond Solid in Two Dimensions: Evidence for Logarithmic Corrections to Scaling*, Phys. Rev. Lett. **104**, 177201 (2010).

[10] K. Harada, T. Suzuki, T. Okubo, H. Matsuo, J. Lou, H. Watanabe, S. Todo, and N. Kawashima, *Possibility of Deconfined Criticality in SU(N) Heisenberg Models at Small N*, Phys. Rev. B **88**, 220408 (2013).

[11] S. Pujari, K. Damle, and F. Alet, *Néel-State to Valence-Bond-Solid Transition on the Honeycomb Lattice: Evidence for Deconfined Criticality*, Phys. Rev. Lett. **111**, 087203 (2013).

[12] R. Kaul and A. Sandvik, *Lattice Model for the SU(N) Néel to Valence-Bond Solid Quantum Phase Transition at Large N*, Phys. Rev. Lett. **108**, 137201 (2012).

[13] G. Murthy and S. Sachdev, *Action of Hedgehog Instantons in the Disordered Phase of the (2 + 1)-Dimensional CP^{N-1} Model*, Nucl. Phys. **B344**, 557 (1990).

[14] R. K. Kaul and S. Sachdev, *Quantum Criticality of U(1) Gauge Theories with Fermionic and Bosonic Matter in Two Spatial Dimensions*, Phys. Rev. B **77**, 155105 (2008).

[15] M. A. Metlitski, M. Hermele, T. Senthil, and M. P. A. Fisher, *Monopoles in CP^{N-1} Model via the State-Operator Correspondence*, Phys. Rev. B **78**, 214418 (2008).

[16] F. J. Jiang, M. Nyfeler, S. Chandrasekharan, and U. J. Wiese, *From an Antiferromagnet to a Valence Bond Solid: Evidence for a First-Order Phase Transition*, J. Stat. Mech. (2008) P02009.

[17] K. C. Y. Huang, Y. Deng, A. B. Kuklov, N. V. Prokof'ev, and B. V. Svistunov, *Deconfined Criticality Flow in the Heisenberg Model with Ring-Exchange Interactions*, Phys. Rev. Lett. **110**, 185701 (2013).

[18] O. I. Motrunich and A. Vishwanath, *Comparative Study of Higgs Transition in One-Component and Two-Component Lattice Superconductor Models*, arXiv:0805.1494.

[19] A. B. Kuklov, M. Matsumoto, N. V. Prokof'ev, B. V. Svistunov, and M. Troyer, *Deconfined Criticality: Generic First-Order Transition in the SU(2) Symmetry Case*, Phys. Rev. Lett. **101**, 050405 (2008).

[20] L. Bartosch, *Corrections to Scaling in the Critical Theory of Deconfined Criticality*, Phys. Rev. B **88**, 195140 (2013).

[21] A. Banerjee, K. Damle, and F. Alet, *Impurity Spin Texture at the Critical Point between Neel-Ordered and Valence-Bond-Solid States in Two-Dimensional SU(3) Quantum Antiferromagnets*, Phys. Rev. B **83**, 235111 (2011).

[22] F. Alet, G. Misguich, V. Pasquier, R. Moessner, and J. L. Jacobsen, *Unconventional Continuous Phase Transition in*

a Three-Dimensional Dimer Model, Phys. Rev. Lett. **97,** 030403 (2006).

[23] S. Powell and J. T. Chalker, *SU*(2)-*Invariant Continuum Theory for an Unconventional Phase Transition in a Three-Dimensional Classical Dimer Model,* Phys. Rev. Lett. **101,** 155702 (2008).

[24] D. Charrier, F. Alet, and P. Pujol, *Gauge Theory Picture of an Ordering Transition in a Dimer Model,* Phys. Rev. Lett. **101,** 167205 (2008).

[25] S. Powell and J. T. Chalker, *Classical to Quantum Mapping for an Unconventional Phase Transition in a Three-Dimensional Classical Dimer Model,* Phys. Rev. B **80,** 134413 (2009).

[26] G. Chen, J. Gukelberger, S. Trebst, F. Alet, and L. Balents, *Coulomb Gas Transitions in Three-Dimensional Classical Dimer Models,* Phys. Rev. B **80,** 045112 (2009).

[27] D. Charrier and F. Alet, *Phase Diagram of an Extended Classical Dimer Model,* Phys. Rev. B **82,** 014429 (2010).

[28] R. K. Kaul, *Quantum Criticality in SU*(3) *and SU*(4) *Antiferromagnets,* Phys. Rev. B **84,** 054407 (2011).

[29] S. Ferrara, R. Gatto, and A. F. Grillo, *Positivity Restrictions on Anomalous Dimensions,* Phys. Rev. D **9,** 3564 (1974).

[30] G. Mack, *All Unitary Ray Representations of the Conformal Group SU*(2, 2) *with Positive Energy,* Commun. Math. Phys. **55,** 1 (1977).

[31] E. Brézin and J. Zinn-Justin, *Finite Size Effects in Phase Transitions,* Nucl. Phys. **B257,** 867 (1985).

[32] J. March-Russell, *On the Possibility of Second-Order Phase Transitions in Spontaneously Broken Gauge Theories,* Phys. Lett. B **296,** 364 (1992).

[33] J. L. Cardy and H. W. Hamber, *O*(*n*) *Heisenberg Model Close to n = d = 2,* Phys. Rev. Lett. **45,** 499 (1980).

[34] F. D. M. Haldane, *O*(3) *Nonlinear σ Model and the Topological Distinction between Integer- and Half-Integer-Spin Antiferromagnets in Two Dimensions,* Phys. Rev. Lett. **61,** 1029 (1988).

[35] N. Read and S. Sachdev, *Valence-Bond and Spin-Peierls Ground States of Low-Dimensional Quantum Antiferromagnets,* Phys. Rev. Lett. **62,** 1694 (1989).

[36] N. Read and S. Sachdev, *Some Features of the Phase Diagram of the Square Lattice SU*(*N*) *Antiferromagnet,* Nucl. Phys. **B316,** 609 (1989).

[37] A. Nahum, J. T. Chalker, P. Serna, M. Ortuño, and A. M. Somoza, *3D Loop Models and the CP^{n-1} Sigma Model,* Phys. Rev. Lett. **107,** 110601 (2011).

[38] A. Nahum, J. T. Chalker, P. Serna, M. Ortuño, and A. M. Somoza, *Phase Transitions in 3D Loop Models and the CP^{n-1} Sigma Model,* Phys. Rev. B **88,** 134411 (2013).

[39] R. K. Kaul, R. G. Melko, and A. W. Sandvik, *Bridging Lattice-Scale Physics and Continuum Field Theory with Quantum Monte Carlo Simulations,* Annu. Rev. Condens. Matter Phys. **4,** 179 (2013).

[40] T. A. Bojesen and A. Sudbø, *Berry Phases, Current Lattices, and Suppression of Phase Transitions in a Lattice Gauge Theory of Quantum Antiferromagnets,* Phys. Rev. B **88,** 094412 (2013).

[41] See, e.g., Fig. 9 of Ref. [28], which quantifies finite-size corrections to $z = 1$ scaling in the SU(3) and SU(4) J–Q models.

[42] J. Cardy, *Quantum Network Models and Classical Localization Problems,* in *50 Years of Anderson Localization,* edited by E. Abrahams (World Scientific, Singapore, 2010).

[43] A. M. Ferrenberg and R. H. Swendsen, *New Monte Carlo Technique for Studying Phase Transitions,* Phys. Rev. Lett. **61,** 2635 (1988); *Optimized Monte Carlo Data Analysis,* Phys. Rev. Lett. **63,** 1195 (1989).

[44] J. Cardy, *Scaling and Renormalization in Statistical Physics* (Cambridge University Press, Cambridge, England, 1996).

[45] The $(\vec{\phi}^2)^2$ theory with an *n*-component field [the O(*n*) model] maps to a loop gas in a standard way [44]. We may ask what the dangerous irrelevance of the quartic term for $d > 4$ means in the language of the loop gas. On scales small compared with the system size, the loops have a well-defined fractal dimension of two. The naive expectation from scale invariance would be that at the critical point, the number of spanning strands is $O(1)$, so the total length of these "long" strands is $O(L^{d_f}) = O(L^2)$. This is violated as a result of the dangerous irrelevance of the quartic term. Instead, the total length of long loops is $O(L^{d/2})$—one can calculate the full joint probability distribution for the lengths of the long loops using the method of Ref. [46]—and the spanning number is of order $L^{d/2}/L^{d_f} = L^{(d-4)/2}$. This also gives the scaling of the spin stiffness (defined using the response to infinitesimal twists of the boundary conditions). We see that it diverges at the critical point, rather than taking a finite universal value.

[46] A. Nahum, J. T. Chalker, P. Serna, M. Ortuño, and A. M. Somoza, *Length Distributions in Loop Soups,* Phys. Rev. Lett. **111,** 100601 (2013).

[47] This measurement probes the fractal structure of loops on scales smaller than the system size. An alternative is to attempt a scaling collapse of the total length of system-spanning strands versus the number of such strands (more precisely, of NL^{3-d_f} against the spanning number $\mathcal{N}_s$ defined in Sec. IV C; data not shown). This gives similar results: $\eta_{\text{Néel}} \sim 0.42$ if small L values are included in the fit, falling to $\eta_{\text{Néel}} \sim 0.31$ when sizes less than $L = 250$ are dropped.

[48] $\chi_{\text{VBS}} = N_{\text{sites}}^{-1}(\langle \vec{\phi}^2 \rangle - \langle |\vec{\varphi}|^2 \rangle)$.

[49] K. Vollmayr, J. D. Reger, M. Scheucher, and K. Binder, *Finite Size Effects at Thermally-Driven First Order Phase Transitions: A Phenomenological Theory of the Order Parameter Distribution,* Z. Phys. B **91,** 113 (1993).

[50] J. Lou, A. Sandvik, and L. Balents, *Emergence of U*(1) *Symmetry in the 3D XY Model with Z$_q$ Anisotropy,* Phys. Rev. Lett. **99,** 207203 (2007).

[51] M. S. Block, R. G. Melko, and R. K. Kaul, *Fate of CP^{n-1} Fixed Points with q Monopoles,* Phys. Rev. Lett. **111,** 137202 (2013).

[52] T. Senthil and M. P. A. Fisher, *Competing Orders, Nonlinear Sigma Models, and Topological Terms in Quantum Magnets,* Phys. Rev. B **74,** 064405 (2006).

[53] A. Tanaka and X. Hu, *Many-Body Spin Berry Phases Emerging from the π-Flux State: Competition between Antiferromagnetism and the Valence-Bond-Solid State,* Phys. Rev. Lett. **95,** 036402 (2005).

[54] This formulation [52] is a sigma model that groups the Néel and VBS order parameters into a single five-component vector. It includes a Wess-Zumino-Witten term, and

anisotropy terms that break SO(5) symmetry for rotations of this vector. If the transition was continuous and the anisotropies (with the exception of the operator driving the transition) happened to be irrelevant, SO(5) symmetry would emerge at large scales. This might be more surprising in $2 + 1D$ than in $1 + 1D$ [55] since, in the absence of any symmetry-breaking terms, the SO(5) sigma model (with the WZW term) already has one stable fixed point, which is the ordered phase. If we postulate another stable critical fixed point, then we must also postulate an unstable multicritical point in between. However, this cannot be ruled out.

[55] This is described by the $SU(2)_1$ Wess-Zumino-Witten model, which has an emergent SO(4) symmetry that rotates the dimerization and the three components of the Néel vector into each other [56].

[56] A. M. Tsvelik, *Quantum Field Theory in Condensed Matter Physics*, 2nd ed. (Cambridge University Press, Cambridge, England, 2003).

[57] A. Nahum, P. Serna, J. T. Chalker, M. Ortuño and A. M. Somoza, arXiv:1508.06668.

[58] With open BCs, $\langle \mathcal{N}_s \rangle$ is identical to the stiffness defined in the usual way by the response of the free energy to an infinitesimal twist in the BCs for the Néel vector [38,59]. Here, we use periodic BCs and define $\mathcal{N}_s$ by slicing open the system. This means that $\langle \mathcal{N}_s \rangle$ is no longer simply related to the free energy but does not change the qualitative scaling behavior.

[59] A. Nahum, P. Serna, A. M. Somoza, and M. Ortuño, *Loop Models with Crossings*, Phys. Rev. B **87**, 184204 (2013).

[60] In general, in a finite system with a single hedgehog, the absolute phase depends on the boundary conditions for $\vec{z}$. With periodic BCs, we have an equal number of hedgehogs and antihedgehogs. An antihedgehog (of opposite topological charge) has the opposite phase.

[61] M. Levin and T. Senthil, *Deconfined Quantum Criticality and Néel Order via Dimer Disorder*, Phys. Rev. B **70**, 220403 (2004).

[62] R. K. Kaul, *Quantum Phase Transitions in Bilayer SU(N) Anti-ferromagnets*, Phys. Rev. B **85**, 180411 (2012).

[63] It is also now clear that the scaling violations are not due to fourfold anisotropy in the VBS order parameter (see Refs. [7,11,51] and Sec. IV B), so their explanation should be sought in the framework of the NCCP^1 model.

[64] In addition to the loop model, lattice field theories, and quantum Hamiltonians (and variants [7,11]) mentioned so far, scaling violations are seen in the ordering transition of the 3D classical dimer model, which is also argued to be described by the NCCP^1 model [23–27]. In that model, there is potentially an additional complication due to higher-order terms in the action that break SU(2) symmetry.

[65] B. I. Halperin, T. C. Lubensky, and S.-K. Ma, *First Order Phase Transitions in Superconductors and Smectic-A Liquid Crystals*, Phys. Rev. Lett. **32**, 292 (1974).

[66] I. D. Lawrie and C. Athorne, *Phase Transitions in Non-linear Abelian Higgs Models*, J. Phys. A **16**, L587 (1983).

[67] S. Hikami, *Three-Loop β-Functions of Non-Linear σ Models on Symmetric Spaces*, Phys. Lett. B **98**, 208 (1981).

[68] S. Hikami, *Renormalization Group Functions of CP^{N-1} Non-Linear σ-Model and N-Component Scalar QED Model*, Prog. Theor. Phys. **62**, 226 (1979).

[69] A. Nahum and J. T. Chalker, *Universal Statistics of Vortex Lines*, Phys. Rev. E **85**, 031141 (2012).

[70] The derivative of $n_*(d)$ has in fact also been calculated in the limit $d \to 4$ by going to next leading order in the epsilon expansion: $(dn_*/dd)|_{d=4} \simeq 320.2$: see Ref. [71]. Note that, contrary to the suggestion in Ref. [71], we have argued that the inverted XY fixed point at $n = 1$, $d = 3$ is not continuously connected to the fixed points accessible via $4 - \epsilon$ or large n (Sec. VI C).

[71] F. Herbut and Z. Tesanovic, Phys. Rev. Lett. **78**, 980 (1997)

[72] The merging with the tricritical point occurs when a scaling variable becomes marginal. In the NLSM, the only candidates that preserve the symmetry are operators with more than two derivatives. Those with four derivatives have RG eigenvalues of the form $y = f(t^*) - d$, where t_* is the sigma model coupling at the critical point [73]. Therefore, t_* is $O(1)$ at the point where $y = 0$. For small ϵ, the coupling t_* is of order ϵ/n. This indicates that $n_*(2 + \epsilon) \propto \epsilon$ as stated in the text. Since t_* is $O(1)$ in the regime of interest, lowest-order calculations do not fix the coefficient of proportionality.

[73] I. V. Lerner and F. Wegner, *High-Gradient Operators of the Unitary Matrix-Model*, Z. Phys. B **81**, 95 (1990).

[74] J. L. Cardy, M. Nauenberg, and D. J. Scalapino, *Scaling Theory of the Potts-Model Multicritical Point*, Phys. Rev. B **22**, 2560 (1980).

[75] One may also consider the RG equation for the leading thermal scaling variable which drives the transition. Very close to the merging line, we can approximate this as $d\mu/d \ln L = (y + b\lambda)\mu$ (similarly to, e.g., Refs. [38,74]), which gives one way to define an effective $\nu = (y + b\lambda)^{-1}$ that drifts with λ.

[76] λ will appear to be a conventional marginally irrelevant variable only when $\lambda \gtrsim |\Delta|^{1/2}$, so that the second term in Eq. (27) dominates. For example, defining L_* as the scale where $\lambda^2 = |\Delta|$ gives $L_* \sim \xi^{1/4}$.

[77] C. Dasgupta and B. I. Halperin, *Phase Transition in a Lattice Model of Superconductivity*, Phys. Rev. Lett. **47**, 1556 (1981).

[78] The assumption is often made in the literature that the scaling dimensions of monopole insertion operators interpolate smoothly, as a function of n, between the value at the inverted XY transition and in the large n regime. In light of the above, this assumption is not justified.

[79] E. V. Herland, T. A. Bojesen, E. Babaev, and A. Sudbø, *Phase Structure and Phase Transitions in a Three Dimensional SU(2) Superconductor*, Phys. Rev. B **87**, 134503 (2013).

[80] For more about the phase diagram in the limit $n \to 1$, see Ref. [69].

[81] M. Kamal and G. Murthy, *New O(3) Transition in Three Dimensions*, Phys. Rev. Lett. **71**, 1911 (1993).

[82] The reasons given here for the failure of the $2 + \epsilon$ expansion of the O(3) model should not be confused with earlier speculations that for any fixed ϵ, operators with a very large number of derivatives may become relevant and destabilize

the fixed point. Reference [83] has argued that such speculations are not well founded.

[83] E. Brézin and S. Hikami, *Irrelevance in the $(d-2)$ Expansion of Nonlinear σ and Heisenberg Models*, Phys. Rev. B **55**, R10169 (1997).

[84] E. Brézin and J. Zinn-Justin, *Renormalization of the Nonlinear σ Model in $2+\epsilon$ Dimensions—Application to the Heisenberg Ferromagnets*, Phys. Rev. Lett. **36**, 691 (1976).

[85] E. Fradkin, D. A. Huse, R. Moessner, V. Oganesyan, and S. L. Sondhi, *Bipartite Rokhsar-Kivelson Points and Cantor Deconfinement*, Phys. Rev. B **69**, 224415 (2004).

[86] Consider the 3D XY model at its *tricritical* point. This is described by a $(\vec{\phi}^2)^3$ theory at its upper critical dimension. The relevant fixed point is free, but the $(\vec{\phi}^2)^3$ interaction is dangerously (marginally) irrelevant since it is required to cut off the fluctuations of the zero mode of $\vec{\phi}$. The usual duality of the XY model gives a mapping to the single-component Abelian Higgs model (describing a superconductor). The tricritical point of the XY model must be dual to a tricritical point of the Abelian Higgs model (describing a phase transition on the boundary between type I and type II behavior). This tricritical Abelian Higgs model is a strongly interacting theory, but remarkably, it is dual to a free theory, with a dangerously marginally irrelevant perturbation.

[87] P. E. Lammert, D. S. Rokhsar, and J. Toner, *Topology and Nematic Ordering*, Phys. Rev. Lett. **70**, 1650 (1993).

[88] R. K. Kaul, *Spin Nematics, Valence-Bond Solids and Spin Liquids in $SO(N)$ Quantum Spin Models on the Triangular Lattice*, Phys. Rev. Lett. **115**, 157202 (2015).

[89] M. E. J. Newman and G. T. Barkema, *Monte Carlo Methods in Statistical Physics* (Clarendon Press, Oxford, 1999).